Iron Responsive Cell Surface Proteins in *Thalassiosira pseudonana* as Probed
by Biotinylation and Mass Spectrometry

by

Ashley M. New

A thesis submitted to the

Graduate School – Newark

Rutgers, The State University of New Jersey

In partial fulfillment of the requirements

for the degree of

Master of Science

Graduate Program in Environmental Sciences

Written under the direction of

Dr. Adam B. Kustka

and approved by

_____

_____

_____

Newark, New Jersey

May, 2013

Abstract of the Thesis

Iron Responsive Cell Surface Proteins in *Thalassiosira pseudonana* as Probed
by Biotinylation and Mass Spectrometry

By Ashley M. New

Dissertation Director:
Dr. Adam Kustka

We investigated the cell-surface enriched proteome of *Thalassiosira pseudonana* under growth rate limiting (60-70% µ-max) and replete Fe conditions to better understand transporters that may be involved in Fe uptake. High and low Fe cultures were grown in the presence of $^{15}N\text{-}NO_3^-$ (>98%) and $^{14}N\text{-}NO_3^-$ (natural abundance), respectively, enabling relative quantification of proteins. In an effort to identify cell surface proteins, a cell surface labeling and enrichment method was developed and tested. Briefly, cell surface proteins were labeled with a free-amine reactive biotinylation reagent, soluble proteins were removed by membrane lysis and centrifugation, and biotinylated proteins were enriched on a neutravidin resin. Optimal conditions were sought for each of these three processes to increase coverage of cell surface labeled proteins. After elution, extracts were subjected to SDS-PAGE, in-gel tryptic digestion, and separation via liquid chromatography before identification and quantification by tandem mass spectrometry. Identification of cell surface proteins proved problematic due to biotinylation of some intracellular proteins and differential typtic digestion from the presence of the biotin linker arm. We obtained a greater than two-fold

increase in abundance of the plasma membrane iron (III) permease (FTR1)

under low Fe. A second FTR homolog was identified, indicating the presence of

multiple Fe uptake pathways.

Table of Contents

List of Tables & Figures

I. Introduction

    A. Problem Statement

Phytoplankton in the world's oceans account for 48.5 Pg of carbon fixation per year, 46% of global net primary production (Field et al. 1998). While oceans have a lower rate of primary production per unit area (140 g of C m^{-2} $year^{-1}$) compared to terrestrial environments (426 g of C m^{-2} $year^{-1}$), the large area of the oceans results in a high annual rate of carbon fixation (Field et al. 1998). Diatoms account for about 40% of primary production in the ocean, or 25% of global carbon fixation (Falkowski and Raven 1997).

More than 20% of the earth's oceans are described as high nutrient, low chlorophyll (HNLC) (Martin et al. 1994) waters, where chlorophyll concentrations are lower than expected and macronutrients are not depleted. Fe has been found to be the most common limiting nutrient to phytoplankton growth in these systems (Martin et al. 1988; Boyd et al. 2007). Fe enrichment experiments demonstrate that episodic Fe additions lead to community shifts from nanoplankton to blooms of large diatoms (Boyd et al. 2007).

Marine diatoms play a vital role in marine ecosystem structure and function as well as global biogeochemical cycling. Fe availability controls the growth of these marine diatoms in HNLC regions; however, our understanding of Fe acquisition mechanisms remains limited.

B. Objectives

Our objectives were to develop a general method that can be used to accurately distinguish between cell surface proteins and other proteins in marine eukaryotic phytoplankton, with an emphasis on the diatom *Thalassiosira pseudonana* (*T. p.*), and to better understand the Fe responsive cell surface proteome of diatoms in an effort to resolve some outstanding controversies regarding the mechanisms of Fe acquisition in these organisms.

We developed and tested a method to identify and quantify the relative abundances of cell surface proteins from *T. p.* grown under Fe replete and growth rate limiting conditions. First, we tested whether relative quantification of proteins could be obtained by combining isotopic labeling and tandem mass spectrometry (MS/MS) approaches. Then, we tested whether protein tagging with a membrane impermeable reagent combined with MS/MS could be used to identify proteins localized to the cell surface. Based on earlier findings from analyses of *T. p.* transcript abundances (Kustka et al 2007), as well as kinetic considerations (Shaked et al. 2005; Maldonado et al. 2001) we hypothesized that ferric permease (FTR1) and ferric reductase (FRE1) should be cell surface localized and more abundant under low Fe conditions. This approach may also resolve some of the controversies described below, or identify potentially novel proteins involved in Fe transport.

One fundamental limitation of MS/MS methods for identifying and quantifying proteins is that abundant proteins can mask the signals of relatively

rare proteins. Cell surface proteins make up a small fraction of the total proteome. Therefore, cell surface proteins were enriched during sample preparation by labeling these with a cell membrane-impermeable reagent, selectively enriching for membrane proteins by cell lysis and centrifugation, and further retaining labeled proteins through affinity column fractionation. These three steps were optimized to yield the greatest enrichment for these cell surface proteins. First, a suitable ratio between biotinylation reagent and cells was determined by varying this ratio and quantifying the relative yields of biotinylated protein. Second, during membrane fractionation, various physical and chemical disruption methods were tested to reduce the loss of biotinylated proteins and improve removal of soluble intracellular proteins. Third, during affinity column fractionation, the ratio of protein to neutravidin resin was varied to increase the recovery of biotinylated proteins by minimizing non-specific adsorptive losses to the resin.

C. Background and Theory

Different pathways have been proposed for Fe uptake by diatoms. For the better part of two decades, our understanding of Fe acquisition in diatoms and other eukaryotic phytoplankton was dominated by the "Fe prime" ($Fe^/$) model. $Fe^/$ denotes the summed concentrations of all Fe species not complexed by organic ligands. This $Fe^/$ model was established from diatom cultures grown in the presence of various aminocarboxylic acids, which are moderately strong ligands (Hudson and Morel 1990; Sunda and Huntsman 1995). However, when chemical oceanographers first documented the existence of very strong Fe-

binding ligands in the ocean it became clear that equilibrium Fe' is too low to support diatom growth in the most Fe poor HNLC regions (Rue and Bruland 1995; Wu and Luther 1995). This led to the suggestion that Fe reductive processes may be important (Anderson and Morel 1982; Maldonado and Price 2001). An attempt to reconcile the Fe$^{/}$ model with the apparent importance of Fe reduction has led to the Fe(II) cell surface model, which suggests that either Fe$^{/}$ species or ligand bound Fe(III) may be reduced at the cell surface prior to transport into the cell (Shaked et al. 2005).

A reductive-oxidative pathway for Fe acquisition has been characterized in the yeast *Saccharomyces cerevisiae*. In this model (Figure 1) Fe(III) is reduced extracellularly to Fe(II) by membrane reductases (FRE1 and FRE2), reoxidized by a multicopper oxidase (FET3) and directly transferred to a cooperative iron permease (FTR1) which transports the Fe(III) into the cell (Eide 1998; Shi et al. 2003). Yeast FET3 contains only one transmembrane domain, so it is unlikely to enable transport. Amino acid mutations to the predicted transport domains of FTR1 eliminate Fe(III) uptake into the cell, demonstrating its necessity in the reductive-oxidative pathway (Eide 1998). The co-expression of FET3 and FTR1 is supported by mutant knock out studies, which show that the absence of either protein causes the other protein to be mislocalized to other parts of the cell rather than to the cell surface (Eide 1998). Homologs to FRE1 and FTR1 have been found to be transcriptionally upregulated under low Fe (Kustka et al 2007; Whitney et al. 2011; Thamatrakoln et al. 2012). A study of this model in *Thalassiosira oceanica* (T. o.) suggested that Fe transport may require the re-

oxidation of Fe(II) to Fe(III) (Maldonado and Price 2001). This would be consistent with the tight coupling of ferric reductase with a Fe(III) transporter protein, based on Fe reduction and Fe uptake rates, under low Fe in T. o. (Maldonado and Price 2001) and *T. p.* (Kustka et al. 2005; Shaked et al. 2005). It is important to recall that yeast and diatoms thrive in very different environments, so it is likely that Fe uptake may be controlled by yet undescribed mechanisms.

The *T. p.* genome also contains a myriad of non-specific divalent metal transporters that may be responsible for Fe(II) uptake, including those in the NRAMP (natural resistance associated macrophage protein) and ZIP (zinc iron-permease) families. For example, ZIP family Fe transporters in *Aribidopsis thaliana* and *Lycopersicon esculentum* also transport Cd, Co, Mn, and Zn (Eide et al. 1996; Eckhardt et al 2001). Various NRAMP transporters in mammalian and *Chlamydomonas reinhardtii* cells transport a selection of divalent metals, including Fe^{3+}, Zn^{2+}, Mn^{2+}, Co^{2+}, Cd^{2+}, Cu^{2+}, Ni^{2+} and Pb^{2+}, to varying extents (Gunshin et al. 1997; Rosakis and Koster 2005). The internalization of Fe produced by reductases either by the ferroxidase/permease complex or by direct divalent metal transport are consistent with all aspects of the cell surface Fe(II) model. Lane et al. (2008) found T. o. greatly increases Fe(II) uptake under low Fe conditions, but the presence of Cd(II) correspondingly reduces the increase, indicating relatively non-specific divalent metal transporters may be involved (2008). Moderate increases in Fe(III) uptake, which were not affected by the presence of Cd(II) in the media, were also observed under low Fe conditions

(Lane et al. 2008). This indicates high affinity uptake of Fe(III), such as occurs with the reductive-oxidative pathway, which is only moderately upregulated under low Fe conditions (Lane et al. 2008). These results suggest multiple Fe uptake pathways are present and may be utilized in different proportions under different nutrient conditions. Transcripts of *T. p.* NRAMP, a non-specific transporter also significantly increase under low Fe, and decrease significantly within 3 hours of Fe addition (Kustka et al. 2007). A variety of nonspecific and/or Fe specific pathways for Fe uptake could be present in *T. p.*

Several transcripts homologous to known metal uptake proteins have been determined to be upregulated under low Fe conditions (Kustka et al. 2007; Whitney et al. 2011; and Thamatrakoln et al. 2012). However, gene expression does not necessarily correlate with protein abundance (Gygi et al. 1999), and not all metal transport proteins are targeted to the cell surface. Localization studies have revealed this in the case of FET5 and FTH1, which are both localized to the vacuolar membrane in *S. cervisiae* (Urbanowski and Piper 1999). However, the required reverse genetic tools in diatoms are only in their infancy (Poulsen et al. 2006; De Riso et al. 2009). Tagging the cell surface proteins with a biotinylation reagent prior to lysing the cells allows identification of those proteins exposed to the external milieu (Palenik and Koke 1995; Davis et al. 2005). So, we enriched, identified, and quantified cell-surface proteins under steady state low and replete Fe conditions to identify low Fe induced proteins potentially involved in transport.

Liquid chromatography combined with tandem mass spectrometry (LC/MS/MS) enables the identification of proteins in complex samples. After

separation based on size (or other physiochemical parameters) and tryptic digestion, peptides are loaded onto a liquid chromatography column and separated based on charge or hydrophobicity. Separation by LC reduces the complexity of each portion of sample put through the MS, reducing the likelihood of abundant proteins masking less abundant ones (Mann et al. 2001). 'Gentle' methods such as electrospray and matrix-assisted laser desorption ionization (MALDI) enable ionization of large molecules such as peptides (Mann et al. 2001). Ionized peptides are transferred to the MS which measures the mass to charge (m/z) ratio of the peptides (using time-of-flight (TOF), quadrupole electric fields, or ion trap selection) and a signal intensity proportional to the number of ions of each m/z value (Mann et al. 2001; Aebersold and Mann 2003). This relationship differs among peptides due to inherent differences in ionization efficiency. Abundant parent ions are selected for subsequent collision with an inert gas (causing dissociation), and the resulting fragments are introduced to a second MS to determine the m/z of each peptide fragment (Mann et a.l 2001). The m/z ratio of these fragments is compared against a database of known protein sequences in the sample, such as an expressed sequence tag (EST) data base or the species genome, to identify the amino acids in each fragment and the protein the peptide is from (Mann et al. 2001).

A variety of methods have been developed to enable both relative and absolute quantitation of proteins using MS/MS. Absolute quantification of abundant proteins can be obtained by adding known quantities of exogenous proteins to a sample as standards (Silva et al. 2005). For relative quantification

stable isotope tags of N15, C13, or O18 are introduced to proteins by chemical reactions, or as amino acids or nutrient salts to living cells (Aebersold and Mann 2003; Yates et al. 2009). The resultant heavy or light (but otherwise chemically identical) peptides are differentiated in the MS due to the differences in peptide mass (Aebersold and Mann 2003). The ratio of heavy to light ions detected for each protein are statistically compared to determine relative abundance of the protein under two conditions (Yates et al. 2009).

To better understand the Fe responsive cell surface proteome, a method for enriching cell surface proteins has been adapted for *T. p.* as described below. First, cell surface proteins are chemically tagged to enable enrichment and identification of tagged proteins. Multiple options for protein labeling have been described in the literature. The N-hydroxysuccinimide ester of some reagents covalently reacts with the free amine of lysine, while maleimide reagents covalently bond with the thiol group of reduced cystines, and diazobenzoyl biocytin reacts with the phenolic and imidazole groups of tyrosine and histidine, respectively. We tested the Sulfo-NHS-SS-biotin reagent as the hydroxysuccinimide-amine reaction has a pH optimum of ~8.3. The sulfonate moiety prevents diffusion across the membrane, and the disulfide bond allows for elution from the neutravidin resin enrichment using DTT while leaving a linker arm on the protein that may be identified in MS/MS. This reagent is stable and reactive at pH 8 (similar pH to live *T. p.* cultures) and does not require the reduction of cysteine disulfide bonds prior to labeling.

Cell surface labeling was combined with fractionation techniques to enable the identification of proteins which are relatively rare compared to many intracellular proteins. After labeling, the sample was fractionated to enrich for membrane bound proteins. The cells were lysed by resuspending pellets in a detergent to release and solubilize the intracellular portion of the cell. The samples were centrifuged and the supernatant containing the soluble fraction was discarded. The pellet, containing the insoluble membranes, organelles, and frustules, was retained. After multiple washes, the pellet was lysed in a harsher extraction buffer, with sonication, to solubilize the remaining membrane bound proteins, and centrifuged again to remove any remaining insoluble such as the silicon frustules. Avidin-biotin affinity resin fractionation was used to enrich for cell surface proteins. The biotinylated proteins bind to the neutravadin resin, while other, non-labeled, intracellular membrane proteins (i.e. nuclear, mitochondrial, chloroplastic) retained in the membrane fractionation are preferentially washed from the sample. By combining membrane and affinity fractionation, the sample was enriched for the biotin-tagged membrane fraction of the cells.

II. Methods

Samples of *T. p.* were processed to enrich for cell surface proteins through a series of fractionation steps outlined in Figure 2. In brief, *T. p.* was cultured under steady state Fe limited conditions, with a ^{14}N-nitrate (natural abundance) source, while iron replete cultures were grown in ^{15}N-nitrate to allow for relative quantification of low Fe responsive proteins using MS/MS. These cultures were

mixed, sampled with gentle filtration, and treated with the biotinylation reagent. SYTOX green staining was used to ensure that less than 3% of cells were compromised during this stage. Centrifugation was used to collect the membrane fraction, after sequential treatments with cell lysis buffer. Membrane bound proteins were then solubilized in a membrane lysis buffer with sonication. The protein extract was then washed on an affinity column where the biotin tag binds to a neutravadin resin. Then the sample was eluted with DTT to collect the biotinylated proteins. This sample was sent to the MS/MS facility for SDS-PAGE, tryptic digestions, and LC/MS/MS.

A. Culturing

Cultures of *T. pseudonana* (CCMP 1335) were grown in Aquil medium using chelexed Synthetic Ocean Water (Sunda et al. 2005). Media was buffered with 100 µM EDTA and Zn, Mn, Co, Cu, Mo, Se were added at concentrations of 79.7, 121, 50.3, 19.6, 100, and 100nM to achieve inorganic ion concentrations, expressed as $pMe^{/}$, or the negative log of 10.93, 8.03, 10.77, 12.63, 7.00, 8.00, respectively (Sunda et al. 2005) as calculated in Visual MINTEQ. Fe was supplied at either 600 or 100 nM total concentration (for $pFe^{/}$ of 9.57 and 10.69). For replete and growth rate limiting conditions, cultures were grown with NO_3^{-} supplied as ^{15}N (>98%) and ^{14}N (natural abundance), respectively. All cultures were acclimated to these conditions in 28 mL polycarbonate tubes. Steady state growth was confirmed when growth rates differed by <10% upon successive transfers. Growth rates were determined by daily measurements of in-vivo chlorophyll a fluorescence (Turner 10-AU fluorometer). After a minimum of 10

generations of steady state growth, cultures were scaled to larger volumes and cells counts were obtained with a Multisizer 3 Coulter Counter (Beckman-Coulter, Fullerton, CA, USA). Growth rates were calculated as the slope of the linear regression of the natural log of relative fluorescence or cell density over time. Cultures were grown at 18°C and constant light (350 μE m^{-2} s^{-1}) using GE Ecolux white fluorescent bulbs.

B. Cell Surface Sampling

T. p. cultures were grown to ~300,000 cells/mL, and filtered with low vacuum on 3 μm polycarbonate filters. Filtered cells were kept wet and rinsed 2 times with 10 mL chelexed SOW, and then suspended in varying volumes of chelexed SOW with 10 mM NaHCO$_3$. Biotinylation reagent (BR), quenching solution, Tris Buffered Saline (TBS), neutravidin resin, spin columns, and DTT were obtained from the Pierce Cell Surface Protein Isolation Kit (Life Technologies, Cat# 89881). Cell suspensions were mixed with BR as described below. After a 20 minute incubation with gentle shaking at room temperature, quenching solution was added to each treatment. Cells were gently filtered, and rinsed 2 times with 10 mL TBS (20mM Tris, 500mM NaCl, pH 7.5) to remove any excess BR.

C. SYTOX Green Staining

Samples were subjected to SYTOX green (Life Technologies, Cat# S7020) staining according to the vendor's protocol after the BR was quenched to evaluate the amount of cell lysis during biotinylation. Sub-samples were taken

before filtration and after BR quenching to compare native amounts of compromised membrane integrity to those caused by the filtration. Positive control samples were created by adding 1% glutaraldehyde, and negative control samples were collected from the culture before filtering. A Zeiss Axiovert 200 was used with a CHLA (Chroma 31017a) filter to observe cells based on chlorophyll fluorescence and a FITC/EGFP (Chroma 41001) filter for observing SYTOX Green bound to DNA. Any samples which exhibited more than 3% of cells with compromised membranes (SYOTX green positive) were discarded.

D. Biotinylation

If the mole quantity of BR is not saturating, increasing the ratio of cells to BR would increase the amount of labeled cell surface protein and improve identification and quantification results. After filtration, aliquots of cell suspension (in 10 mM $NaHCO_3$, pH 8.0-8.5) were mixed into BR for final concentrations of 0.396mM (sulfo-NHS-SS-biotin) and 10 mM ($NaHCO_3$), pH 8.0-8.5. Eight different concentrations of cells were added to BR, ranging from 1.5E13 – 3.6E14 cell·mol BR^{-1} (Table 1) to optimize the ratio of cell number to moles of BR. To determine which reaction ratio yielded the most biotinylated protein, extracts were lysed in cell lysis buffer (CLB, 50mM Tris, pH 8, 1% SDS, 1 mM EDTA, 100mM PMSF, and 50mM iodoacetamide (IAM)) with sonication, precipitated, dot blotted, and subject to a streptactin-HRP assay to detect biotin (methods described below). Based on these results, subsequent samples were biotinylated under Treatment H (Table 1) conditions with 1.5E13 cell·mol BR^{-1} or 3E8 cells (1.5E8 cells of each Fe treatment) in a 50mL reaction.

E. Membrane Fractionation

In order to enrich for the membrane fraction, cells were resuspended in CLB augmented with either 0.02%, 0.05%, or 0.1% Triton X-100, 0.005% or 0.3% DDM, 0.03% Digitonin, 0.1% SDS, no detergent (all tested with sonication) or 1% SDS gentle shaking and no sonication (Table 2). These were then incubated at room temperature for 30 minutes with gentle shaking, centrifuged at 12,000xg for 10 minutes. The supernatant was removed, and the pellets flash frozen in liquid nitrogen. This clearing was repeated for up to 5 total washes, when chlorophyll was absent from the cell pellet.   Removal was evaluated visually by inspecting supernatants and pellets for relative chlorophyll levels. 0.1% SDS and 0.02% Triton X-100 with sonication and 1% SDS without sonication were selected for further testing as the most likely candidates for effective cell breaking with less solubilization of membrane bound proteins.

The retention of biotinylated proteins during cell lysis was evaluated under these three conditions. Biotinylated samples were subjected to fractionation with 0.02% Triton X-100 with sonication for 4 washes, 0.1% SDS with sonication for 2 washes, and 1% SDS with shaking only for 5 washes, based on the earlier chlorophyll loss results. The resultant suspensions were extracted (described below), then centrifuged. The supernatant was removed, and subsequently precipitated in acetone (described below) to remove detergent from the sample. The samples were resuspended in a low detergent buffer (LDB, 0.05% SDS, 1 mM EDTA, 50 mM Tris, pH 8). Dot blots of these precipitated supernatants and final sample extracts were made to determine the relative amount of biotinylated

protein. Quantifications were determined by analyzing dot blot images with ImageJ software. Samples were stored at -80°C (less than 3 months) until further processing.

F. Membrane Protein Extraction

To solubilize cell surface proteins from the membrane fraction, the pellets were sonicated in 400 uL of membrane lysis buffer (MLB) containing 50 mM Tris, pH 8, 1% SDS, 1% TritonX-100, 1 mM EDTA, 100 mM PMSF, and 50 mM IAM (Branson Sonifier 150, setting 4, 7 seconds on and 8 seconds off, for one min, repeated 4 times with 1 min cooling time between repeats). The samples were centrifuged 12,000xg for 10 minutes to remove frustules and other insoluble material, and the supernatant was collected.

G. Protein Precipitation

Protein samples were precipitated prior to dot blotting or quantification using QBQCA method to remove detergents from the sample. 200 uL of each sample were added to 1.8 mL of pre-chilled acetone, and kept at -20°C overnight to precipitate proteins. Samples were centrifuged with 12,000xg for 10 minutes. The supernatants were discarded, and the protein pellets dried under a HEPA hood for 2 hrs to remove all acetone. The protein pellets were resuspended in 200 uL of LDB (0.05% SDS, 1 mM EDTA, 50 mM Tris, pH 8). Sample were mixed at 3000 RPM for 10 minutes using an Eppendorf MixMate, and then heated to 37°C for 10 min in a water bath. This was repeated 5 times to solubilize as much of the protein as possible.

H. Dot Blotting

First, proteins were loaded onto a nitrocellulose membrane pre-wetted in

Tris Buffered Saline (TBS, 20 mM Tris, 500mM NaCl, pH 7.5). Biotinylated-BSA

standards and precipitated extracts reconstituted in LDB were diluted in LDB to

load the total mass of standard or volume of extract indicated in Figure 3 onto the

BioRad Bio-Dot Microfiltration apparatus. 50 uL of each sample mix was loaded

into each well and gravity filtered onto the membrane. Low vacuum pressure

was used to remove remaining volume after 60 minutes. 50 uL TBS was added

to each well and gravity filtered to wash. Low vacuum pressure was used to

remove remaining volume after 40 minutes.

Next, the membrane was treated with StrepTactin-HRP conjugate to bind

to the biotinylated proteins. The membrane was first blocked in 4% non-fat dry

milk in Phosphate Buffered Saline (PBS), pH 7.2 for 1 hour, then washed 2 times

in PBS for 10 min each, incubated in 1:30,000 StrepTactin-HRP conjugate in 1%

non-fat dry milk in PBS for 1.25 hrs, then washed 6 times in PBS for 10 min

each. HRP conjugate was detected using the Immun-Star HRP

Chemiluminescent Kit with Thermo Scientific CL-XPosure X-ray film in the dark

room. Films were scanned to create a digital copy for image analysis.

I. Protein Quantification

Proteins were quantified using a modified Lowry assay with the BioRad

RC DC Protein Assay kit or Molecular Probes CBQCA Protein Quantitation Kit

and analyzed with the Varion Cary 3E UV-Vis Spectrometer, or Tecan plate

reader, respectively. CBQCA quantification was used when samples were predicted to contain less than 0.2mg/mL protein, while the modified Lowry assay was used for samples predicted to contain higher concentrations.

J.   Affinity Resin Fractionation

Column fractionation should enrich the relative amount of biotinylated proteins, reduce overall sample complexity, and potentially lead to more robust detection and quantification of rare CSPs. However, inherent losses of total protein during this fractionation may negate any advantages gained by reducing sample complexity. Neutravidin agarose spin columns were used to further enrich for biotinylated proteins. The columns were rinsed twice with 1mL of wash buffer (WB) comprised of 50mM Tris, pH 8, 1% SDS, 1% Triton X-100, 1mM EDTA, and 50 mM IAM. To test for optimal retention and recovery of biotinylated proteins a biotinylated sample was split into 4 treatments consisting of 5.67, 2.83, 1.42 mg/mL protein/resin and no column washing (Table 3). The columns were capped securely and gently shaken for 1 hour at room temperature to bind biotinylated proteins to the neutravidin resin. Columns were centrifuged at 1,000xg to remove excess MLB. To remove proteins that were not biotinylated the columns were then washed 4 times with 500uL of WB, centrifuging for 1min at 1,000xg to remove the WB. 400 uL of resin elution buffer (REB) containing 62 mM Tris, pH 6.8, 1% SDS, and 50 mM DTT was added to each column, the columns capped securely and gently shaken at room temperature for 1 hour for the cleavage of the disulfide bond of Sulfo-NHS-SS-biotin, eluting the biotinylated proteins. Columns were centrifuged 2 minutes at 1,000xg and the eluent

collected. 65 mM IAM was added to all 4 samples and incubated in the dark, at room temperature, for 30 min to alkylate thiol groups and prevent crosslinking of proteins. 50 mM DTT was added to quench excess IAM. Samples were flash frozen in liquid nitrogen and stored at 80°C until further processing. These samples were submitted to CABM for SDS-PAGE, tryptic digestion and LC/MS/MS.

K. Cell Surface Processing of Fe Treatments

Two samples were collected and processed for MS/MS. First, a preliminary sample (B5) was biotinylated with 1.5E13 cell·mol BR^{-1} and was subject to affinity column fractionated with about 0.32 mg of protein per mL of settled resin. Notably, no membrane fractionation was performed. This sample was separated via SDS-PAGE, cut into 5 bands, for tryptic digestion and loaded for LC/MS/MS as 5 samples. A second sample (B13) was biotinylated with 1.5E13 cell·mol BR^{-1}, membranes were fractionated twice in CLB with 1% SDS with gentle shaking and centrifugation, and affinity column treatments were varied as described above. These were each subjected to SDS-PAGE for a brief time to load the samples into the gel, followed by in gel tryptic digestion of 1 band for each treatment. Each of the 4 treatments was loaded separately for LC/MS/MS, as a single sample.

L. Mass Spectrometry

Protein extracts were subjected to SDS-PAGE, in-gel tryptic digestion, separation via Dionex U-3000 nano LC system, and Thermo LTQ-Orbitrap-Velos

mass spectrometry. Samples were processed at the Biological Mass Spectrometry Facility of the UMDNJ-Robert Wood Johnson Medical School and Rutgers, The State University of New Jersey. For quantification, data was searched using Proteome Discoverer software. For identification of modifications the data was searched using The Global Proteome Machine software. All searches used the *T. p.* genome (Armbrust et al. 2004).

Quantification of proteins was determined by the ratio of heavy to light peak areas (H:L ratio) of each peptide. Only proteins with 2 or more quantifiable peptides, all with H:L ratios varying less than 25% from one another, were considered.   For each protein, H:L ratios of all component peptides were averaged. H:L protein ratios from each sample were normalized to the median of that sample. This helps account for any systematic differences in the quantification of ^{15}N versus natural abundance labeled peptides, as occurs with isotopic enrichment less 100% and/or with contamination of ^{15}N treatments with bioavailable, natural abundance, nitrogen sources. Proteins were determined to be significantly over or under-represented in a sample if they varied more than 2-fold between treatments. Isotopic H:L ratios of each proteins from the two samples (B5 and B13) were averaged. Proteins with a mean ratio representing a 2-fold or greater change (log2(Normalized N15/N14) > 1) in both biological samples were considered to be significantly over or under represented in both samples. Proteins with a 2-fold or greater difference between Fe treatments, but only quantified in one biological sample were reported as significantly over or under represented in one sample.

M. Statistics

Intracellular protein labeling with the biotin linker arm is detected even in populations of healthy cells, where ≤ 3% of cells are compromised during sampling, suggesting biotinylated peptides cannot be used as de facto evidence of cell surface localization. To determine a threshold metric, we evaluated the biotinylated peak area ratio (BPAR) for peptide pairs of known intracellular proteins. Here peptide pairs are peptides of the same amino acid sequence, differing only by the presence of a biotinylation linker arm. By comparing observed BPARs to the values for known intracellular proteins, proteins could be assigned as cell surface localized if any one ratio is significantly higher than those of known intracellular proteins, as shown in Eq. 1, where T_{crit} is determined with a 1 tailed α of 0.05.

$$Eq. 1 \qquad BPAR_{cell\,surface} \geq \overline{BPAR}_{intracellular} + (T_{crit} \times \sigma_{intracellular})$$

III. Results

A. Method Development

i. Concentration of Biotinylation Reagent

Dot blotting for the presence of biotin in the cell extracts shows that the biotinylation signal was invariant, regardless of cell number per mole BR (Figure 3 & 4). This indicates that the proteins present at a stoichiometry of 1.5E13 cell·mol BR^{-1} (or 3E8 cells / 50 mL) saturate the BR. Therefore, greater yields of biotinylated proteins may be achieved with additional biotinylation reagent but not more cells.

ii. Membrane Fractionation

0.1% Triton X-100 and 0.3% DDM were very effective at breaking cells, with only slight amounts of green color in the pellet after only 1 round (84 seconds). We reasoned that the complete loss of intracellular proteins in the first round of processing with these detergents may be too harsh and solubilize many membrane bound proteins. Three treatments (1% SDS with shaking, 0.1% SDS and 0.02% Triton X-100 with sonication) resulted in more gradual loss of intracellular proteins (within the first 2, 4, and 4 cycles, respectively) as shown in Figure 5. The other treatments all left significant green coloration in the pellet even after 4 rounds (336 seconds) of sonication. 0.1% SDS with sonication, 0.02% Triton X-100 with sonication, and 1% SDS with gentle shaking were selected for further testing as the most likely candidates for effective cell breaking with less solubilization of membrane bound proteins.

Further tests for retention of biotinylated proteins with these three lysis regimes revealed a 40% loss of biotinylated proteins due to 1% SDS, while there was 70% loss of biotinylated proteins due to 0.1% SDS and 0.02% Triton X-100 with sonication (Table 4, Figure 6 & 7). Protein quantification of the supernatants showed that most of the protein loss from the 1% SDS treatment occurred in the first wash, with only about 10% as much in the second wash and concentrations below the detection limit (0.2mg/mL) in subsequent washes. Therefore, since washing samples twice by shaking in CLB with 1% SDS resulted in only a ~25% loss of biotinylated protein and the nearly complete loss of intracellular proteins, this treatment was used in all subsequent samples.

iii. Affinity Resin Fractionation

Column fractionation greatly improved the number of biotinylated proteins identified (59 ± 4.4 versus 22), regardless of the resin/protein stoichiometries tested here (Table 5, Figure 8), compared to the treatment where column fractionation was omitted. This indicates that fractionation on the column reduces the complexity of the sample and enriches for biotinylated proteins, thus increasing the number of identified biotinylated proteins. The identification of both the biotinylated and non-biotinylated proteins found in each of the 4 treatments varied. 23 biotinylated proteins were found in all 4 treatments, and another 24 in common in all 3 of the resin treatments (Figure 9). The high, medium, low, and no column treatments led to the identification of 8, 15, 17, and 4 unique proteins, respectively due to the variability of MS/MS. A total of 174 proteins were found in all 4 treatments and 169 were unique to the no column treatment (Figure 10).

B. Proteomic Analysis

i. Cell Surface Localization

Of 32 known intracellular, non-ribosomal, proteins that were identified in both samples (selected at random), 6 and 16% were biotinylated in sample B5 and B13, respectively (Table 12). Significant but variable percentages of ribosomal proteins were also biotinylated (2 and 42% in sample B5 and B13, respectively) (Table 11). Ribosomal proteins are more likely retained during membrane fractionation steps than are soluble proteins, and they may be prone

to biotinylation due to endocytosis of the biotinylation reagent and their possible location in the endoplasmic reticulum.

The presence or absence of biotinylated peptides from intracellular proteins may not be the most robust metric for discriminating between bona fide cell surface proteins and intracellular proteins that are adventitiously labeled. Even with low percentages of SYTOX-permeable cells, it is not surprising that some peptides of abundant proteins (such as RuBisCO large or small subunits) would be biotinylated. Therefore, we compared the BPAR of peptide pairs (differing only by the presence of the biotinylation mass modification of lysine by 145.01900 amu) for known intracellular proteins and those of unknown localization. Samples B5 and B13 had 16 and 58 proteins with biotinylated peptides. Of these, 10 and 33 proteins had peptide pairs (Table 7) amenable to comparison.

Populations of peptide pairs from intracellular proteins (based on the lack of a SignalP predicted signal peptide cleavage site) and from proteins of unknown localization in sample B5 and B13 had biotinylation ratios (Table 7) of 0.37 ± 0.25 and 0.49 ± 0.23, respectively (Figure 11). Due to the low number of comparable peptide pairs, values from both biological samples we combined for further analysis. Given the distribution of BPAR of peptides of intracellular proteins, a single peptide would need to have a BPAR greater than 0.81 (BPAR > 0.47 + 1.70*(0.25)). Three proteins meet this criterion (a probable serine protease, a predicted protein, and an actin-like protein, Table 8). The first two proteins have predicted signal peptide cleave sites, indicating localization at the

cell surface. However, the third has no predicted signal cleave site, and so was considered intracellular in calculation of the BPAR threshold.

ii. Fe Responsive Protein Quantification

A total of 435 proteins were quantified under low and high Fe conditions, 250 and 304 proteins in B5 and B13, respectively (Table 13). Relative quantifications were obtained for 73 proteins common to both biological samples, varying by less than 25% between the samples. An additional 46 proteins were quantified in both samples but varied by >25%. Proteins that are more differentially expressed are more likely to have variable $^{15}N/^{14}N$ ratios, as small changes in extreme values will have a larger impact on the ratio. Therefore, Fe responsive relative quantifications of all proteins, along with their mean and standard deviation if found in both biological samples, are considered (Table 13).

Most proteins did not exhibit significant changes in abundance between low and high Fe conditions. One protein, FTR1 ferric permease (plasma membrane permease), was overexpressed (log2(Normalized N15/N14) < -1) under iron limiting conditions in both samples (shown in red (Figure 12, Table 9)). Proteins over-represented in low Fe in one replicate, but not quantified in the second (pink) include an ABC transporter, alkaline phosphatase, histone, iron starvation induced, ribosomal, PGR5-like, sterol regulatory element-binding protein, synaptobrevin, and 4 predicted proteins (Table 10). Two proteins, a glutamine dependent carbamoyl phosphate synthase like protein and a pyruvate carboxylase, were over-represented in iron replete conditions in both treatments

(dark blue). Other proteins only over-represented (log2(Normalized N15/N14) > 1) in one replicate under high Fe condition (but not quantified in the second; light blue), include Mg-protoporphyrin chelatase, 3 copper induced cell-surface proteins, DNA-directed RNA polymerase, glutamate 1-semialdehyde 2,1-aminomutase, glycine decarboxylase, nickel-binding ABC transporter, cytoplasmic phosphoenolpyruvate carboxylase, 2 proteins similar to low CO_2 inducible membrane proteins, scp/tpx-1/ag5/pr-1/sc7 domain-containing, and 6 other predicted proteins of unknown function.

iii. Fe Permease and Reductase

FTR1 is over-represented under low Fe conditions in both biological samples. Relative changes in abundance (log2 = -1.06 and -1.93, in B13 and B5, respectively) vary from about a 2-fold, to about a 4-fold increase in FTR1. However, FRE1, the ferric reductase protein, was not quantified. The protein may be present in the sample, but not in high enough abundance for detection via MS/MS or is not ionizable. FTR1 is biotinylated in both B5 and B13.

IV. Discussion

Natural cell death, as well as sample processing, may release some intracellular proteins prior to and during biotinylation. Consequently, some amount of intracellular protein is inevitably tagged with the biotinylation reagent. With the current approach, there is significant overlap among the biotinylation ratios of peptide pairs from known intracellular proteins and other potential or putatively described cell surface proteins. In future studies, additional steps can

be taken to potentially increase the signal of biotinylated bona fide cell surface proteins relative to the background of biotinylated intracellular proteins. Cell number was not limiting the biotinylation reaction, so increasing the amount of biotinylation reagent used could increase labeling of cell surface proteins. Similarly, further optimization of membrane fractionation could result in the retention of biotinylated proteins greater than the 75% we have achieved here. Optimizing affinity column fractionation increased the identification of biotinylated peptides and proteins by 3-fold, but this type of fractionation reduces the sensitivity of the BPAR metric. The BPAR potentially differentiates between intracellular and cell surface biotinylated proteins based on the assumption that a large percentage of accessible lysine residues for cell surface proteins will be biotinylated while, at most, 3% of intracellular proteins could be biotinylated due to compromised cell membranes. During affinity column fractionation both cell surface and intracellular biotinylated proteins will increase in relative abundance within the sample, as non biotinylated proteins are washed from the sample. A greater proportion of intracellular proteins are not biotinylated, and so their ratio of biotinylated to non-biotinylated proteins will increase more than that of cell surface proteins.

In the absence of affinity column fractionation, with simplifying assumptions, the BPAR for intracellular and cell surface peptides can be described in Eq. 2 and 3, respectively.

$$Eq.2 \qquad BPAR = \delta IE \times SH \times A$$

δIE indicates differential ionization efficiency between peptide pairs (driven solely by the presence of the biotinylation linker arm), which is assumed to be 1 as relative abundance only relates to peak areas when IE is the same. SH of biotinylation indicates the steric hindrance of an individual lysine residue to biotinylation (the lower the value, the less accessible the lysine is to the reagent). The SH value for any given peptide is constant. Accessibility (A) indicates the percentage of lysine residues that could be accessed by the biotinylation reagent (amount of a given peptide exposed to the external milieu vs. amount of the same peptide not exposed to BR). For intracellular proteins, maximum values for A are set at 0.03, while apoplastic lysine residues of extracellular proteins maximum values for A are set at 1.

With affinity resin fractionation, BPAR can be defined by Eq. 3,

$$Eq.3 \qquad BPAR = \ \delta IE \ \times SH \ \times A \ \times AE$$

where affinity enrichment (AE) indicates enrichment through the selective retention of biotinylated proteins. The product of A and AE cannot exceed 1. Therefore, with affinity resin enrichment, the BPAR of intracellular peptides may increase while that of accessible cell surface peptides may not.

As with all MS/MS proteomics not all proteins present are detectable. Low abundance proteins are less likely to be detected. Not all peptides of a protein are ionizable. Therefore, the absence of a protein from the proteome, does not indicate that it may not be present in the cell. Similarly, the lack of a biotin linker arm does not necessarily indicate that a protein is not located at the cell surface.

As not all peptides in a protein are ionizable in the MS, the peptide containing a linker arm may not be detected, even if it is present in the sample (Figure 13). Potential future work could include processing samples for cell surface localization and protein abundance separately. Samples could be biotinylated, membrane fractionated, trypticly digested, and then enriched on a neutravadin affinity column before running on the MS/MS. This would enhance the identification of biotinylated peptides, but few proteins would have more than one peptide identified. The quantification and/or identification of a protein require the quantification and/or identification of at least two peptides of that protein. Therefore, future samples may be split for treatment (1) to best identify biotinylated peptides, and (2) to relatively quantify the Fe responsive proteome separately.

The BPARs of intracellular proteins did not create a robust threshold for cell surface localization, as it classified 1 out of 3 proteins with no signal cleavage site as localized to the cell surface. The lack of a predicted signal cleavage site was used to determine if proteins were intracellular. Some cell surface proteins may lack a signal cleavage site if they are complexed to other proteins or associated to the diatom frustule, but these should be relatively rare. Many biotinylated peptides did not have a quantifiable non-biotinylated counterpart. When this occurs, it is unknown if the sample contains lower abundances of non-biotinylated peptides or whether the lack of a linker arm reduces the ionization efficiency of an otherwise similarly abundant peptide. Another problem we discovered is that the biotinylation linker arm attached to lysine residues

interferes with some tryptic cut sites. Therefore, some peptides are cut differentially based on the presence of the linker arm (Figure 14). This may have contributed to the small number of peptide pairs observed in the MS/MS data. Even when a peptide pair is observed, we cannot determine whether the formation of alternate peptides from the same locus is favored due to the presence or absence of the linker arm. If it were, this would change the apparent abundance of one peptide within a peptide pair, and skew the results (Figure 14). Future work should consider proteases that cut at amino acids other than lysine.

Not all cell surface proteins were tagged using the biotinylation of lysine residues with Sulfo-NHS-SS-biotin. Other reagents should be considered for future work targeting Fe transport proteins. Maleimide biotin binds to cysteine residues (pH 6.5-7.5), and diazonenzoyl biocytin reacts with tyrosine and histidine residues (pH 8.4, Mader et al. 2000), either of which may enable the labeling of proteins that do not have an accessible lysine exposed to the external milue.

FTR1 was significantly over-expressed under Fe limiting conditions. This iron permease was also biotinylated, increasing the likelihood of it being localized at the cell surface. However, the BPAR of the FTR1 (0.04) peptide pair did not exceed the threshold value of 0.81, and so it was not designated as cell surface. Previous studies of the proposed reductive – oxidative pathway have shown a tight 1:1 ratio of ferroxidase FET3 with the ferric permease FTR1. The absence of a quantifiable FET3 in the proteome does not mean that it is not present in the cell as it may not be detectable via MS/MS. However, the presence of two ferric

permease proteins, FTR1 and FTR2, indicates another pathway utilizing the second Fe permease either in addition to or instead of a reductive – oxidative pathway.

While the ferric reductace protein FRE was also not quantified, we cannot discount its participation in the reductive-oxidative pathway for Fe uptake, as proteins not quantified may still be present but not detectable. Likewise, NRAMP, the divalent metal transporter transcriptionally upregulated under low Fe was also not found.

Under low Fe there was an at least 2-fold down-regulation of several proteins involved in carbon metabolism, including PEPC (required for C4-type carbon concentration mechanism), the key photorespiratory protein glycine decarboxylase, and proteins involved in the urea cycle (Allen et al. 2011). These observations are consistent with a decreased CO_2 demand relative to flux in Fe-limited cells, as expected with a depressed growth rate. Others in our lab (Colin Gates, senior Honor's thesis) have shown Ni-urease activities are elevated in this diatom grown under low CO_2. It is possible the putative Ni-binding ABC transporter subunit, up-regulated under high Fe, functions to transport Ni into the diatom to satisfy the Ni requirements for urease under conditions of low CO2 flux relative to demand, as would be expected under high growth rate.

V.   Conclusion

Combined membrane and affinity column fractionation effectively increases observed abundances of biotinylated proteins in the sample. Tests to optimize

the sampling and fractionation procedure led to reducing the loss of biotinylated proteins, and increasing the removal of non-biotinylated proteins. This enabled better detection of comparatively rare proteins, such as those in the cell surface membrane. However assignment of proteins as localized to the cell surface proved to be problematic. Further work on BPARs could enable more accurate localization.

FTR1 was found with greater than 2-fold increase in abundance under Fe limiting conditions, and may be localized to the cell surface, supporting the reductive-oxidative pathway. FET3 and FRE1 were not quantified in the Fe responsive proteome; however, their absence may be due to the limitations of MS/MS detection rather than their absence from the cell. While no obvious novel candidates for Fe uptake were observed, an FTR1 homolog was found with a 1.8-fold increase in abundance under low Fe. As FTR1 and FET3 are co-expressed (1:1) in yeast, the presence of different FTR protein indicates a potential second pathway, either at the cell surface, or across an internal plasma membrane. These findings demonstrate the need for further research into Fe uptake mechanism in diatoms.

VI. References

Aebersold, R. & Mann, M., 2003. Mass spectrometry-based proteomics. *Nature*. 422. pp.198-207.

Allen, A.E. et al., 2008. Whole-cell response of the pennate diatom Phaeodactylum tricornutum to iron starvation. *Proceedings of the National Academy of Sciences*, 105(30), pp.10438 –10443.

Anderson, M.A. & Morel, Francois M. M., 1982. The Influence of Aqueous Iron Chemistry on the Uptake of Iron by the Coastal Diatom Thalassiosira weissflogii. *Limnology and Oceanography*, 27(5), pp.789–813.

Armbrust, E.V. et al., 2004. The Genome of the Diatom Thalassiosira Pseudonana: Ecology, Evolution, and Metabolism. *Science*, 306(5693), pp.79 – 86.

Baldauf, S.L., 2003. The Deep Roots of Eukaryotes. *Science*, 300(5626), pp.1703 –1706.

Bowler, C. et al., 2008. The Phaeodactylum genome reveals the evolutionary history of diatom genomes. *Nature*, 456(7219), pp.239–244.

Boyd, P.W. et al., 2007. Mesoscale Iron Enrichment Experiments 1993-2005: Synthesis and Future Directions. *Science*, 315(5812), pp.612 –617.

Clemens S., 2006. Toxic metal accumulation, responses to exposure and mechanisms of tolerance in plants. *Biochimie*, 88(11), pp.1707–1719.

Davis, A.K. et al., 2005. A Stress-Induced Protein Associated with the Girdle Band Region of the Diatom *Thalassiosira pseudonana* (Bacillariopyta). *Journal of Phycology*. 41. Pp.577-589.

De Riso, V. et al., 2009. Gene silencing in the marine diatom *Phaeodactylum tricornutum*. *Nucleic Acids Research*, 37(14) pp.e96.

Eide, D. et al., 1996. A novel iron-regulated metal transporter from plants identified by functional expression in yeast. *Proceedings of the National Academy of Sciences*, 93(11), pp.5624 –5628.

Eide, D.J., 1998. The Molecular Biology of Metal ion Transport in *Saccharomyces cervisiae*. *Annual Review of Nutrition*, 18(1), pp.441–469.

Falkowski, P.G. & Raven, J.A., 2007. *Aquatic Photosynthesis:* 2nd ed., Princeton University Press.

Field, C.B. et al., 1998. Primary Production of the Biosphere: Integrating Terrestrial and Oceanic Components. *Science*, 281(5374), pp.237 –240.

Gunshin, H. et al., 1997. Cloning and characterization of a mammalian proton-coupled metal-ion transporter. *Nature*, 388(6641), pp.482–488.

Hudson, R.J.M. & Morel, François M. M, 1990. Iron transport in marine phytoplanktn: Kinetics of cellular and medium coordination reactions. *Limnology and Oceanography*, 35(5), pp.1002–1020.

Kustka, A.B. et al., 2005. Extracellular Production of Superoxide by Marine Diatoms: Contrasting Effects on Iron Redox Chemistry and Bioavailability. *Limnology and Oceanography*, 50(4), pp.1172–1180.

Kustka, A.B., Allen, A.E. & Morel, François M. M, 2007. Sequence Analysis and Transcriptional Regulation of Iron Acquisition Genes in Two Marine Diatoms1. *Journal of Phycology*, 43(4), pp.715–729.

Lane, E.S. et al., 2008. The interaction between inorganic iron and cadmium uptake in the marine diatom Thalassiosira oceanica. *Limnology and Oceanography*, 53(5), pp.1784–1789.

Mader et al., 2000. S-layer-coated liposomes as a versatile system for entrapping and binding target molecules. *Biochimica et Biophysica Acta (BBA) – Biomembranes,* 1463(1), pp142-150.

Maldonado, M.T. & Price, Neil M, 2001. Reduction and Transport of Organically Bound Iron by Thalassiosira Oceanica (bacillariophyceae). *Journal of Phycology*, 37(2), pp.298–310.

Mann, M., Hendrickson, R.C., & Pandey, A. 2001. Analysis of Proteins and Proteomes by Mass Spectrometry. *Annual Review of Biochemistry*. 70. Pp. 437-473.

Martin, J. H. & et al, 1994. Testing the iron hypothesis in ecosystems of the equatorial Pacific Ocean. *Nature*, 371, pp.123–129.

Martin, John H. & Fitzwater, S.E., 1988. Iron deficiency limits phytoplankton growth in the north-east Pacific subarctic. *Nature*, 331, pp.341–343.

Oliveros, J.C. 2007. VENNY. An interactive tool for comparing lists with Venn Diagrams. http://bioinfogp.cnb.csic.es/tools/venny/index.html.

Palenik, B. & Koke, J.A., 1995. Characterization of a nitrogen-regulated protein identified by cell surface biotinylation of a marine phytoplankton. *Applied and Environmental Microbiology*, 61(9), pp.3311 –3315.

Polsen, N., Chesley, P. M., & Kroger, N., 2006. Molecular genetic manipulation of the diatom *Thalassiosira pseudonana* (Bacillariophyceae). *Journal of Phycology,* 42, pp.1059–1065.

Rosakis, A. & Köster, W., 2005. Divalent metal transport in the green microalga Chlamydomonas reinhardtii is mediated by a protein similar to prokaryotic Nramp homologues. *BioMetals*, 18(1), pp.107–120.

Rue, E.L. & Bruland, K.W., 1995. Complexation of iron(III) by natural organic ligands in the Central North Pacific as determined by a new competitive ligand equilibration/adsorptive cathodic stripping voltammetric method. *Marine Chemistry*, 50(1–4), pp.117–138.

Shaked, Y., Kustka, A.B. & Morel, François M. M., 2005. A General Kinetic Model for Iron Acquisition by Eukaryotic Phytoplankton. *Limnology and Oceanography*, 50(3), pp.872–882.

Shi, X. et al., 2003. Fre1p Cu^{2+} Reduction and Fet3p Cu^{1+} Oxidation Modulate Copper Toxicity in Saccharomyces cerevisiae. *Journal of Biological Chemistry*, 278(50), pp.50309 –50315.

Sunda, W.G., Price, N.M. & Morel, F.M.M., 2005. Trace metal ion buffers and their use in culture studies. *Algal culturing techniques. Elsevier, London, United Kingdom*, pp.35–63.

Sunda, William G. & Huntsman, S.A., 1996. Antagonisms between cadmium and zinc toxicity and manganese limitation in a coastal diatom. *Limnology and Oceanography*, 41(3), pp.373–387.

Sunda, William G. & Huntsman, S.A., 1998. Interactions among Cu^{2+}, Zn^{2+}, and Mn^{2+} in controlling cellular Mn, Zn, and growth rate in the castal alga Chlamydomonas. *Limnology and Oceanography*, 43(6), pp.1055–1064.

Sunda, William G. & Huntsman, S.A., 1995. Iron uptake and growth limitation in oceanic and coastal phytoplankton. *Marine Chemistry*, 50(1–4), pp.189–206.

Urbanowski, J. L. & Piper, R. C., 1999. The Iron Transporter Fth1p Forms a Complex with the Fet5 Iron Oxidase and Resides on the Vacuolar Membrane. *The Journal of Biological Chemistry*. 274(53), pp.38061-38070.

Wu, J. & Luther III, G.W., 1995. Complexation of Fe(III) by natural organic ligands in the Northwest Atlantic Ocean by a competitive ligand equilibration method and a kinetic approach. *Marine Chemistry*, 50(1–4), pp.159–177.

Yates, J.R., Ruse, C.I., Nakorchevsky, A., 2009. Proteomics by Mass Spectrometry: Approaches, Advances, and Applications. *Annual Review of Biomedical Engineering*. 11. pp.49-79.

VII.   Figures and Tables

Figure 1. Reductive-oxidative Fe uptake model, described in the yeast *Sacchomyces cervisiae*. Transcript homologs to the reductase protiens FRE1 and FRE2, the ferroxidase FET3, and ferric permease FTR1 have been found upregulated in *T. p.* under Fe limiting conditions. TMD for *T. p.* protein homologs shown as predicted by TMHMM Server v. 2.0, CBS.
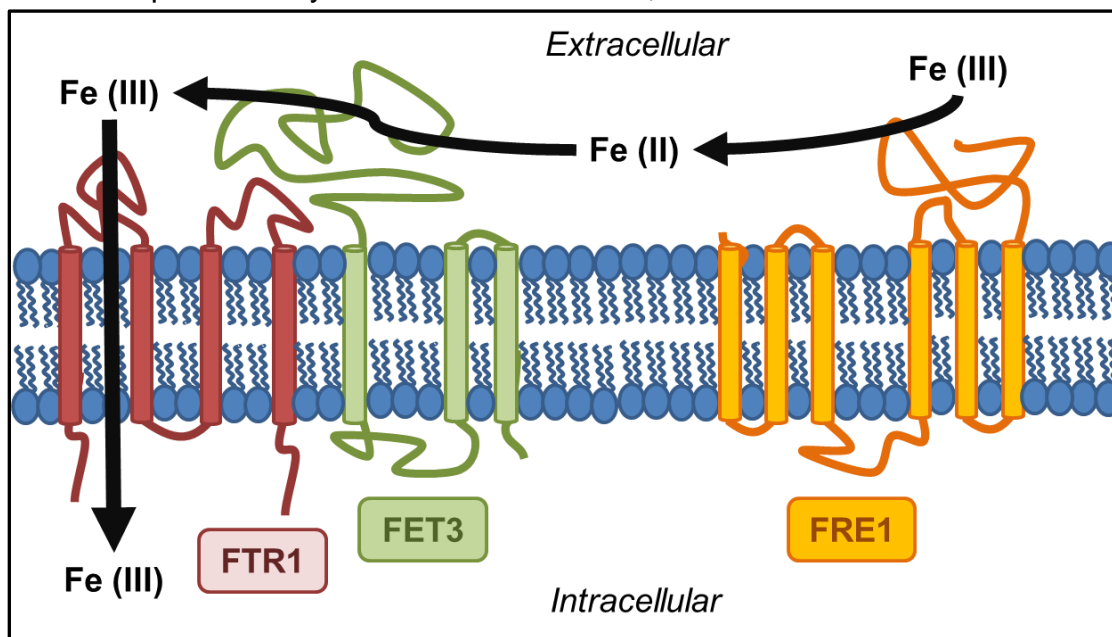
Figure 2. Cell surface protein sampling process. Samples of *T. p.* were processed to enrich for cell surface proteins through a series of fractionation. In brief, *T. p.* was cultured under steady state high iron conditions. Iron limited cultures were grown in an N-14 nitrate source, while iron replete cultures were grown in N-15 nitrate to allow for relative quantification of proteins using mass spec. These cultures were mixed, sampled with gentle filtration, and treated with the biotinylation reagent. SYTOX green staining was used to ensure that less than 3% of cells were compromised during this stage. In a lysis buffer, centrifugation was used to collect the membrane fraction, with repeated washes. Membrane bound proteins were then solubilized in a membrane lysis buffer with sonication. The protein extract was then washed on an affinity column where the biotin tag binds to a neutravadin resin. Then the sample was eluted to collect the cell surface proteins. This sample was sent to the MS/MS facility for SDS-PAGE, tryptic digestions, and LC/MS/MS.
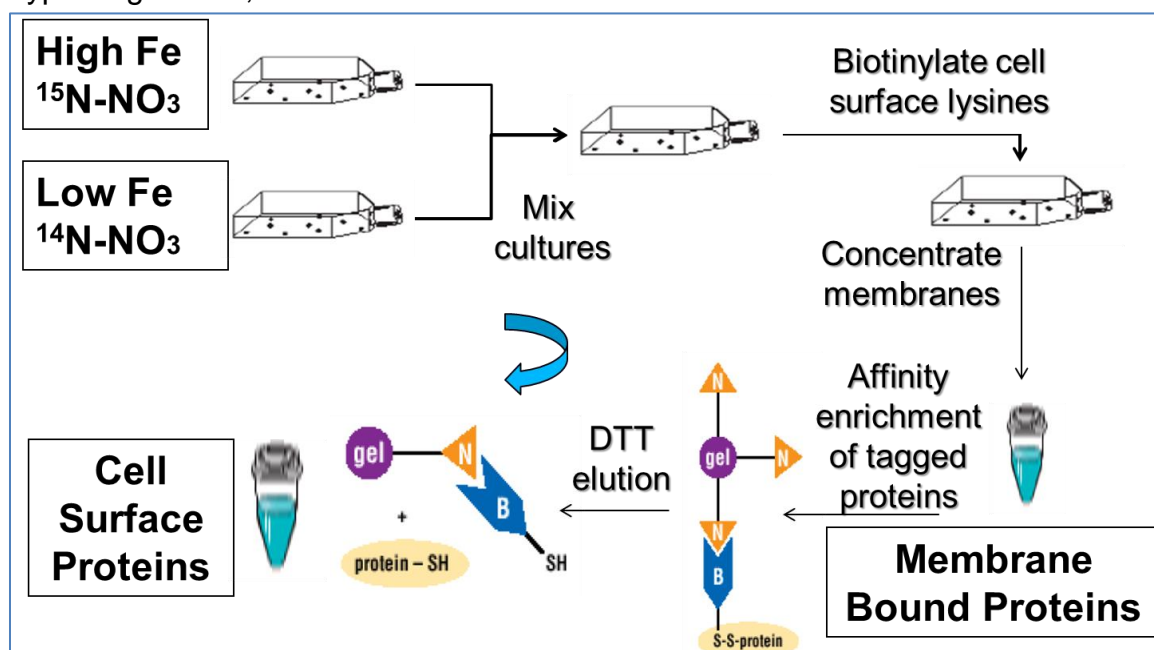
Table 1. Biotinylation efficiency treatments tested.

Treatment	Cell #	Cell Concentration (cells/mL)	Reaction Volume (mL)	[BR] (M)	Reaction Ratio (cells/mol BR)
H	3.00E+08	6.00E+06	50	3.96E-04	1.52E+13
I	3.00E+08	1.20E+07	25	3.96E-04	3.03E+13
J	3.00E+08	3.00E+07	10	3.96E-04	7.58E+13
K	3.00E+08	4.20E+07	7.143	3.96E-04	1.06E+14
D2	4.00E+08	4.22E+07	9.478	3.96E-04	1.07E+14
E	4.00E+08	6.32E+07	6.325	3.96E-04	1.60E+14
F	4.00E+08	9.49E+07	4.216	3.96E-04	2.40E+14
G	4.00E+08	1.42E+08	2.811	3.96E-04	3.59E+14

Table 2. Cell lysis treatments tested.

Physical Disruption	Chemical Disruption	
Sonication	Triton X-100	0.02%
		0.05%
		0.10%
	DDM	0.01%
		0.30%
	Digitonin	0.03%
	SDS	0.10%
Gentle Shaking		1%

Table 3. Affinity column fractionation treatments tested

		Protein/Resin (mg/mL)	Protein (mg)	Settled Resin (mL)	Resin Slurry (uL)
A	Low Resin/Protein	5.67	0.0397	0.028	56
B	Medium Resin/Protein	2.83	0.0397	0.014	28
C	High Resin/Protein	1.42	0.0397	0.007	14
D	No Column Washing	-	0.0397	0	0

Figure 3. Dot blots of concentration biotinylation efficiency test. Standards correspond only to the samples directly above, which are from the same blot. Efficiency of biotinylation reaction remains constant across all treatments (described in Table 1), independent of the cell concentration during the biotinylation reaction.
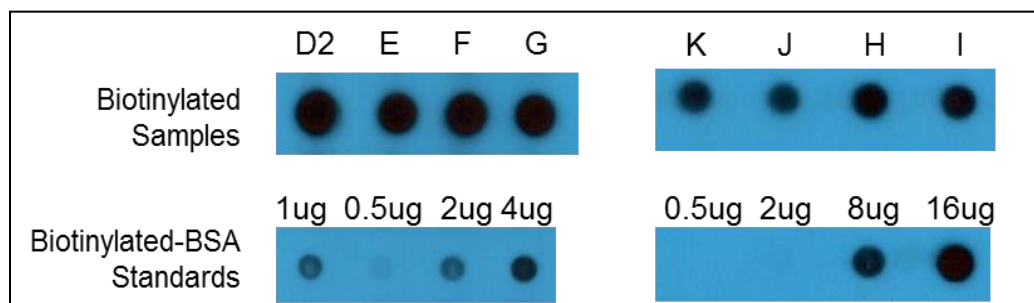
Figure 4. After biotinylation, cell samples were extracted and dot blotted to detect relative concentrations of biotin in the sample with an HRP conjugate. Densitometry with ImageJ software was used to relatively quantify the amount of biotin, and therefore the amount of biotinylated protein in the samples. The biotinylation signal was invariant, regardless of the reaction ratio. This indicates that the proteins present at a stoichiometry of 1.5E13 cell·mol BR^{-1} (or 3E8 cells / 50 mL) saturate the BR.
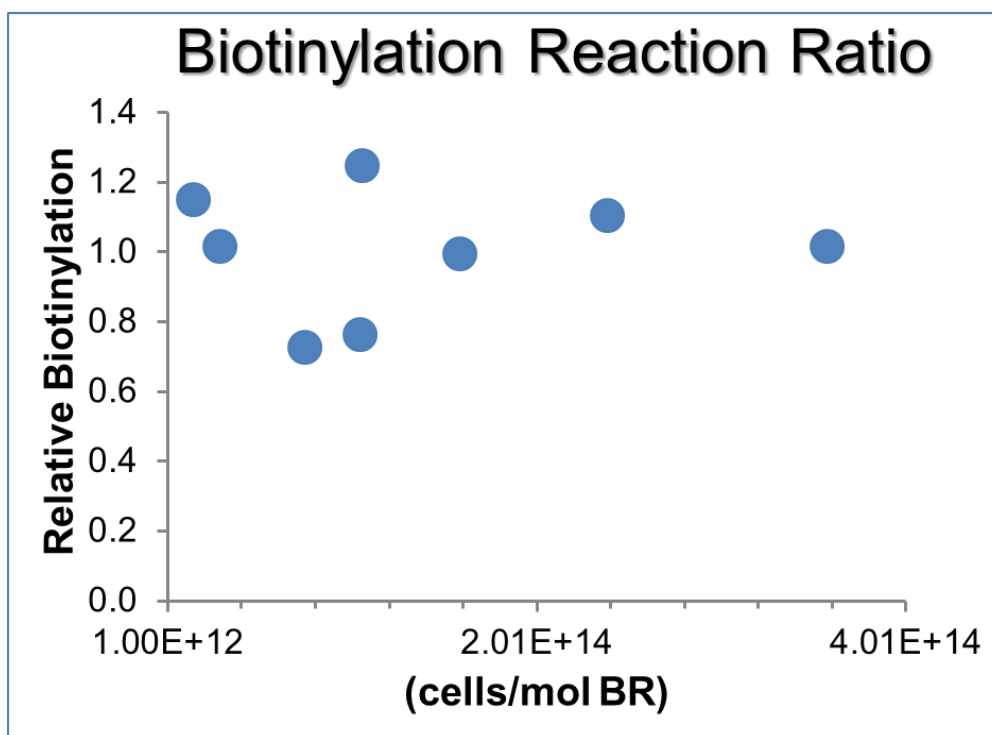
Figure 5. Membrane fractionation test results. Combinations of chemical and physical disruption methods. Relative cell lysis was determinined by visual inspection of chlorophyll remaining in the cell pellet after each wash and centrifugation step. 0.02% Triton X-100 + sonication, 0.1% SDS + sonication, and 1% SDS + shaking showed moderate cell breaking rates, and were selected for further testing.

Physical Disruption	Sonication							Gentle Shaking	
Chemical Disruption	-	Triton X-100			DDM		Digitonin	SDS	
	-	0.01%	0.02%	0.1%	0.005%	0.3%	0.03%	0.1%	1%
Initial									
Wash 1									
Wash 2									
Wash 3									
Wash 4									

Table 4. Protein concentrations, and calculated biotinylated protein concentrations in final membrane-only extracts (M-ex), supernatant from wash (SNx), and whole cell extract (WC-ex).

Treatment			M-ex	SN1	SN2	SN3	SN4	SN5	WC-ex
			Calculated Biotinylated Protein (pg/cell)						
Sonication	Triton X-100	0.02%	195	101	79	78	70	-	10728
Sonication	SDS	0.10%	82	111	85	-	-	-	1686
Shaking	SDS	1%	466	183	121	114	107	86	-
			Total Protein Quantification (mg/mL)						
Sonication	Triton X-100	0.02%	ND	775	ND	ND	ND	-	1060
Sonication	SDS	0.10%	ND	507	ND	-	-	-	1686
Shaking	SDS	1%	ND	670	73	ND	ND	ND	-

Figure 6. Dot blots of membrane fractionation. Blot was loaded with sample equivalent to 0.4uL final membrane-only extracts (M-ex), 4uL supernatant from wash (SNx), and 0.4uL whole cell extract (WC-ex).
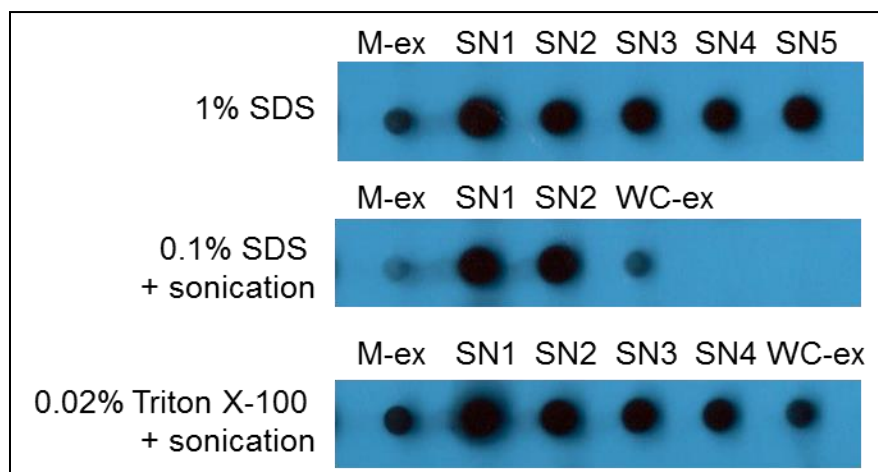
Figure 7. Membrane fractionation test results. Biotinylated cell samples treated with repeated membrane fractionation washes. 1% SDS + shaking, and 0.02% Triton X-100 + sonication retained the most biotinylated protein.
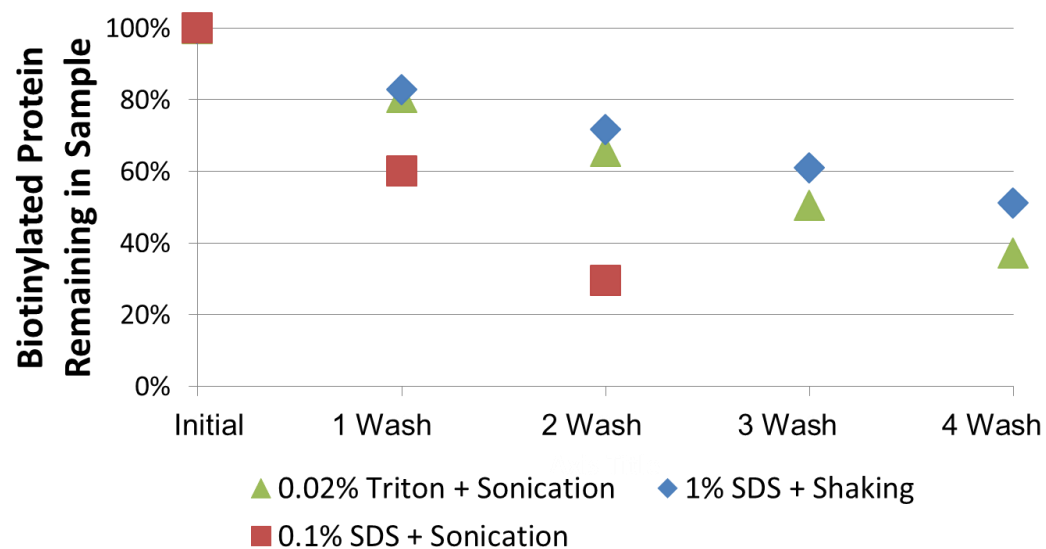
Table 5. Resin loading test. Peptide counts are spectral counts. Tagged proteins are those with at least one lysine modified with the biotinylation reagent linker arm mass. Tagged proteins are proteins with one or more tagged peptides.

	High Protein/Resin	Med Protein/Resin	Low Protein/Resin	No Column
	5.76 mg/mL	2.83 mg/mL	1.42 mg/mL	0 mg/mL
total peptide count	**1986**	**1860**	**2564**	**2404**
# unique peptides	902	876	1155	1319
# unique proteins	197	197	264	373
total tagged peptide count	**284**	**284**	**332**	**112**
# unique tagged peptides	146	153	172	65
# unique tagged proteins	57	56	64	22
% peptides tagged	**14.3%**	**15.3%**	**13.0%**	**4.7%**
% unique peptides tagged	16.2%	17.5%	14.9%	4.9%
% unique proteins tagged	28.9%	28.4%	24.2%	5.9%

Figure 8. Affinity resin fractionation test. Number of total and biotinylated unique proteins quantified from neutravadin resin treatments. Affinity fractionation increases detection of rare biotinylated proteins. Different ratios of protein/resin show similar levels of enrichment.
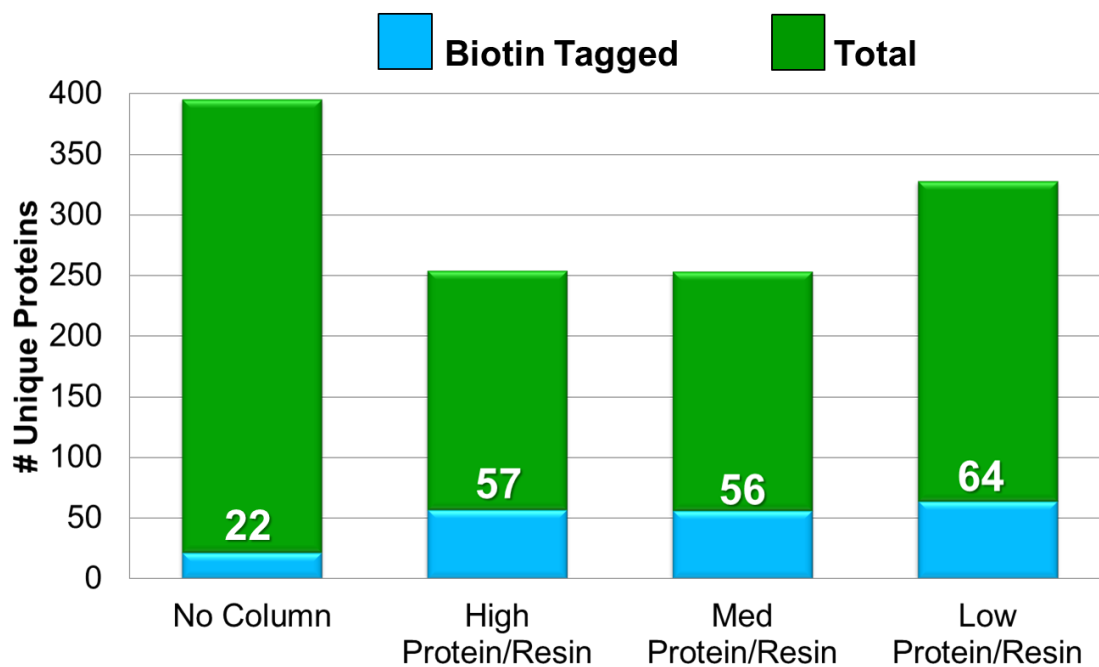
Figure 9. Column fractionation test. Number of biotinylated proteins in each treatment, high, medium and low protein/resin (P:R) ratios and a no resin column treatment. 23 biotinylated proteins were found in all 4 treatments, and 24 in common in all 3 column treatments. Some proteins were unique between treatments due to the variability of MS/MS. Made with Venny (Oliveros 2007).
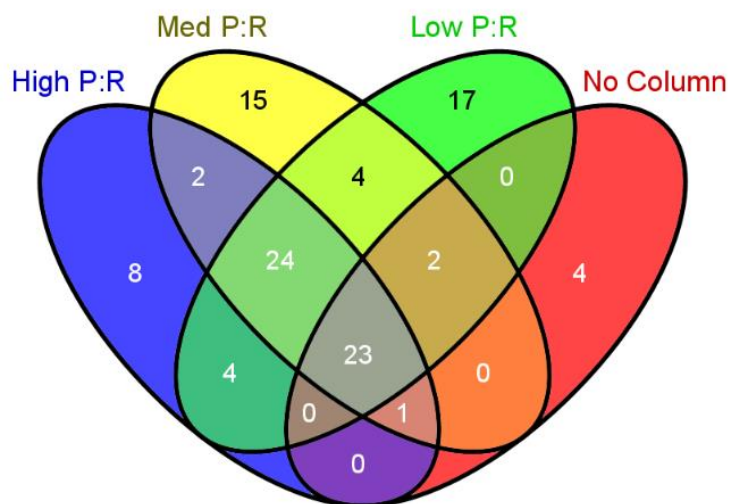
Figure 10. Column fractionation test. Total number of proteins in each treatment, high, medium and low protein/resin (P:R) ratios and a no resin column treatment. 174 proteins were found in all 4 treatments, and 169 proteins were unique to the No Column treatment. Made with Venny (Oliveros 2007).
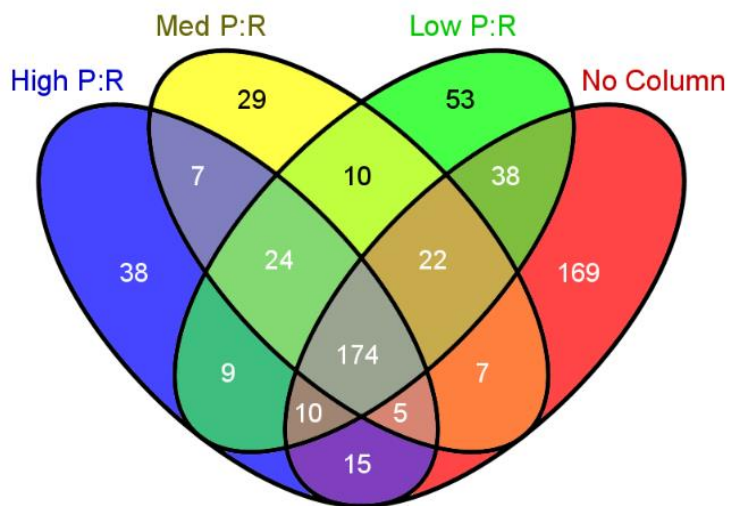
Table 6. Summary if intracellular biotinylation. See Tables 10 and 11 for more data.

Proteins		B5	B13
Intracellular	# Identified	32	32
	# Biotinylated	2	5
	% Proteins Biotinylated	6%	16%
Ribosomal	# Identified	49	55
	# Biotinylated	1	23
	Proteins Biotinylated	2%	42%

Table 7. Biotinylated peptide ratios (Tagged/Total peak ares). Each protein is listed with the number of predicted TMD and SignalP cleavage sites.

	ID	Description	TMD	Signal P	Sequence	Mean	Std Dev
B5	B5YLV5	Predicted protein	1	1	SMcAIAAccDFkNSSEAK	0.74	
					ALVSPYFLkTNPSTATEGIPR	0.31	
					FVDVPVYLkcLDLSGYGPK	0.36	
					KYcSHGAYYTEGNLVNQQK	0.52	0.09
	B8BQL6	Ftr1_plasma membrane iron permease	4	0	LPMALLKPFGYSAGR	0.04	0.03
	B8BTM9	Sterol regulatory element-binding protein	12	0	LAkDEVQGAR	0.45	
					LKTDPEYkDLIK	0.09	
					YSNEIGWDGKK	0.18	
	B8BV60	Predicted protein	1	1	kVATTLHGGLK	0.82	
	B8LE04	Iron starvation induced protein	0	1	FDADTDFkR	0.17	0.01
B13	B5YLX5	copper-induced girdle band-associated cell surface protein precursor	0	1	FVDVPVYLK	0.01	
					IYYkIEGLK	0.57	
					kYcSHGAYYTEGNLVNQQK	0.66	0.01
					kYcSHGAYYTEGNLVNQQkDcDGILVTK	0.70	
					YcSHGAYYTEGNLVNQQkDcDGILVTK	0.31	0.09
					YPDKYDVDELPTPGQTYAHSDGFVQR	0.60	
	B5YLZ3	Predicted protein	0	1	DYVKDEEDAAVK	0.21	
					VSKDYVKDEEDAAVK	0.45	
	B5YMN6	Protein scp/tpx-1/ag5/pr-1/sc7 domain-containing protein	0	0	NkGSGNWGELYDAEK	0.48	0.01
	B5YN94	Protein scp/tpx-1/ag5/pr-1/sc7 domain-containing protein	0	0	LLGGcSGSNLVHAk	0.06	0.05
					SEAFkDDTAcGKPcPNEGcFA	0.11	
	B5YN96	Protein scp/tpx-1/ag5/pr-1/sc7 domain-containing protein	0	0	AEAFKDETGcGDPcPK	0.33	0.34
	B8BR30	Adenine nucleotide translocator; ATP/ADP translocase	2	0	VkLLIQTQDANPK	0.43	

B8BXD7	possible ascorbate peroxidase	0	1	NRcEVSSLENkEcSR	0.41	
				WkDAVALLGAHTLGR	0.59	0.02
B8C0R3	RL13A, ribosomal protein 13A 60S large ribosomal subunit	0	0	AkAEEAAAGDLAK	0.65	0.16
B8C1L0	Cation transporting ATPase (EC 3.6.3.-) (Predicted protein) (Fragment)	8	0	AADALkNmLSTDAR	0.29	
B8C1P3	RS11, ribosomal protein 11 40S small ribosomal subunit	0	0	TPDAAIEGNYVDkK	0.24	
B8C553	Adenosylhomocysteinase (EC 3.3.1.1)	0	0	cKGVSEETTTGVHR	0.56	
B8C6H5	Probable serine protease inhibitor	0	1	kNTYVcFK	0.49	
				kYVGTGSITGTTR	0.74	0.11
B8C788	Probable serine protease inhibitor	0	1	GGSASSckSNEFcAGTDGR	0.56	0.29
B8C789	Probable serine protease inhibitor	0	1	cVNGVkGDLASALR	0.01	
				GGSANSckSNEFcAGTDGR	0.87	0.03
				DkYcQLPTGEcNK	0.39	0.02
				DKYcQLPTGEcNKR	0.45	0.25
				KNSYYcFK	0.43	
				NYVGkGSITSTTK	0.88	0.10
B8C995	Translation elongation factor alpha (EC 3.6.5.3)	0	0	EMDkLQATAEEK	0.63	
B8CB74	Mucin associated surface protein	4	1	AKADQEAAAAAAAK	0.31	
B8CFV4	Actin-like protein	0	0	DAYVGDEAQAkR	0.91	
B8LEN2	Predicted protein	0	1	KNFEcTSGDGVNSVTTHcPNYDPK	0.57	

Table 8. Cell surface proteins, as determined by the BPAR threshold. Peptides with BPARs significantly different (BPAR > 0.81) than the BPAR of intracellular proteins (based on the lack of a Signal P cleave site).

ID	Description	Sequence	BM	SignalP
B8BV60	Predicted protein	kVATTLHGGLK	0.82	1
B8C789	Probable serine protease inhibitor	cVNGVkGDLASALR	0.01	1
		GGSANSckSNEFcAGTDGR	0.87	
		DkYcQLPTGEcNK	0.39	
		DKYcQLPTGEcNKR	0.45	
		KNSYYcFK	0.43	
		NYVGkGSITSTTK	0.88	
B8CFV4	Actin-like protein	DAYVGDEAQAkR	0.91	0

Figure 11. Peptide BPARs from intracellular proteins (based on the lack of a SignalP cleavage site. From this data, a peptide must have a BPAR > 0.81 to be classified as a located at the cell surface.
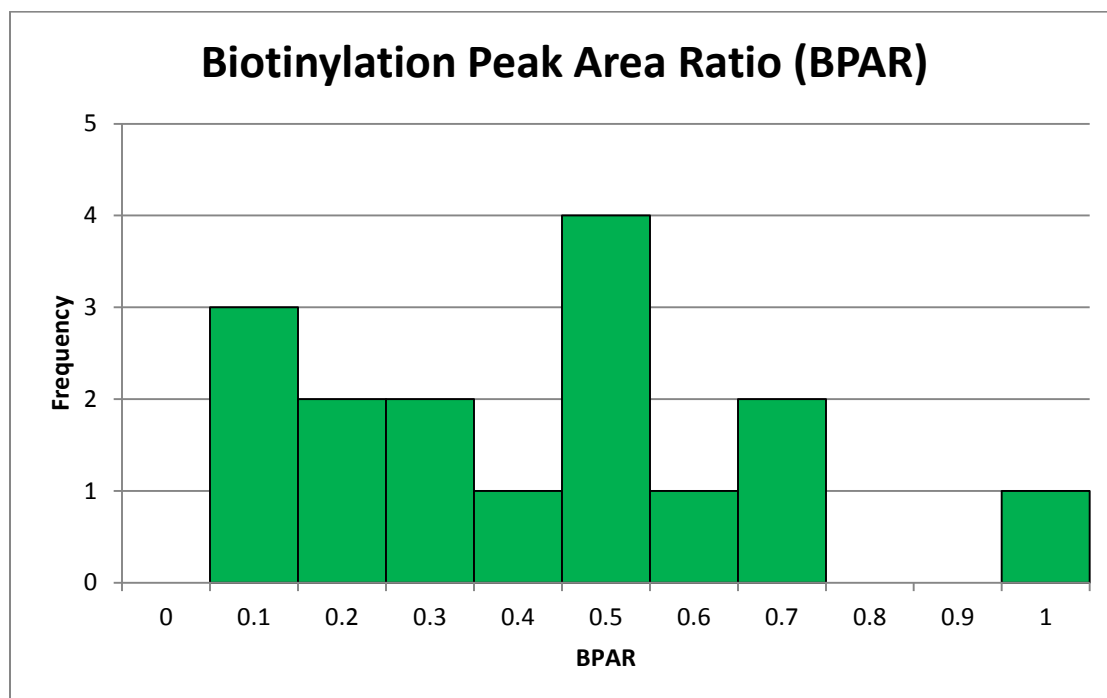
Figure 12. Relative abundances of proteins under low and high Fe between two experiments, expressed as Log2 values of the normalized global $^{15}N/^{14}N$ ratio. Proteins are plotted along the X axis according to alphabetical order of their Uniprot identifications. Proteins over-represented under low Fe conditions are shown in red or pink. Those over-represented under high Fe conditions are shown in dark or light blue, and non-responsive proteins are shown in dark or light grey. The darker hues represent average $^{15}N/^{14}N$ values when quantified in both experiments, and lighter hues represent values when proteins were quantified in only one experiment.
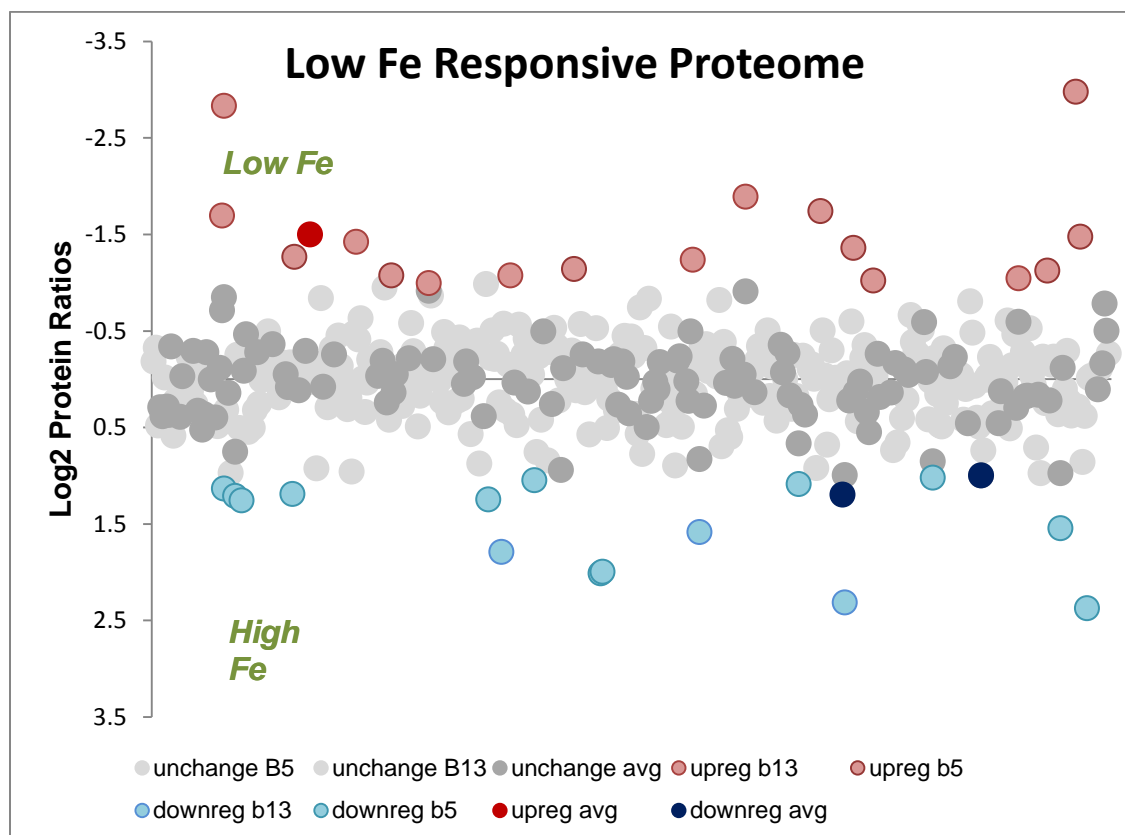
Table 9. Proteins significantly regulated in replicate samples.

ID	Description	Log2(N15/N14)		Mean	SD
		B13	B5		
B8BQL6	Ftr1_plasma membrane iron permease	-1.06	-1.93	-1.50	0.44
B8C8T5	Glutamine dependent Carbamoyl phosphate synthase like protein	1.33	1.07	1.20	0.13
B8CE42	Pyruvate carboxylase-like protein	0.99	1.00	1.00	0.01

Table 10. Relative quantification of proteins significantly changed in one sample.

ID	Description	Log2(N15/N14)	
		B13	B5
B8BQ67	Alkaline phosphatase (EC 3.1.3.1) (Fragment)	-	-1.27
B8BS24	Histone H2A (Fragment)	-1.42	-
B8BTM9	Sterol regulatory element-binding protein	-	-1.07
B8BY22	HNKH	-1.08	-
B8BZQ3	PGR5-like protein	-	-1.14
B8C2A8	Predicted protein	-1.24	-
B8C875	Predicted protein	-	-1.74
B8C8V5	Synaptobrevin (Fragment)	-	-1.36
B8CA11	ABC transporter multi-drug efflux transporter-like protein (Fragment)	-	-1.02
B8CGJ9	40S ribosomal protein S28	-	-1.12
B8LE04	Iron starvation induced protein	-	-2.98
B8LE89	Predicted protein	-	-1.48
A0T0R1	DNA-directed RNA polymerase subunit beta (EC 2.7.7.6) (PEP) (Plastid-encoded RNA polymerase subunit beta) (RNA polymerase subunit beta)	1.16	-
B5YMQ0	Glutamate 1-semialdehyde 2,1-aminomutase	-	1.26
B8BQ15	Chelatase of mg-protoporphyrin IX chelatase	-	1.19
B8BWS1	Predicted protein	1.22	-
B8BX31	Glycine decarboxylase p-protein	-	1.25
B8BYW8	Phosphoenolpyruvate carboxylase (EC 4.1.1.31); cytoplasmic (PEPC)	-	1.05
B8BZ49	Predicted protein	1.18	-
B8C0D8	similar to low CO2 inducible membrane protein	-	2.01
B8C0D9	similar to low CO2 inducible membrane protein	-	2.00
B8C4Q7	Protein scp/tpx-1/ag5/pr-1/sc7 domain-containing protein	1.18	-
B8C7U8	Predicted protein	1.34	-
B8C872	Predicted protein	1.93	-
B8CAS8	Copper induced cell-surface protein	1.12	-
B8CAU5	copper induced cell-surface protein	1.86	-
B8CAV0	Copper induced cell-surface protein	1.46	-
B8CBB2	Protein scp/tpx-1/ag5/pr-1/sc7 domain-containing protein	1.68	-
B8LEL7	Nickel ABC transporter, periplasmic nickel-binding protein	-	2.38
B8LEM7	Predicted protein	1.79	-
B8LEN2	Predicted protein	1.41	-

Figure 13. The absence of a protein from the cell surface proteome does not indicate that it is not part of the cell surface. Not all proteins can be identified with MS. Also, not all peptides of a protein are biotinylated. When only a few peptides are identified, it is likely that the biotinylated peptide may not be. Here two proteins are biotinylated cell surface proteins. Trypsin digestion cuts the proteins into peptides. Ionizable peptides (blue) are identified, but the biotinylated portion of Protein B is not ionizable (white), threfore only Protein A would be deemed as cell surface with the MS.
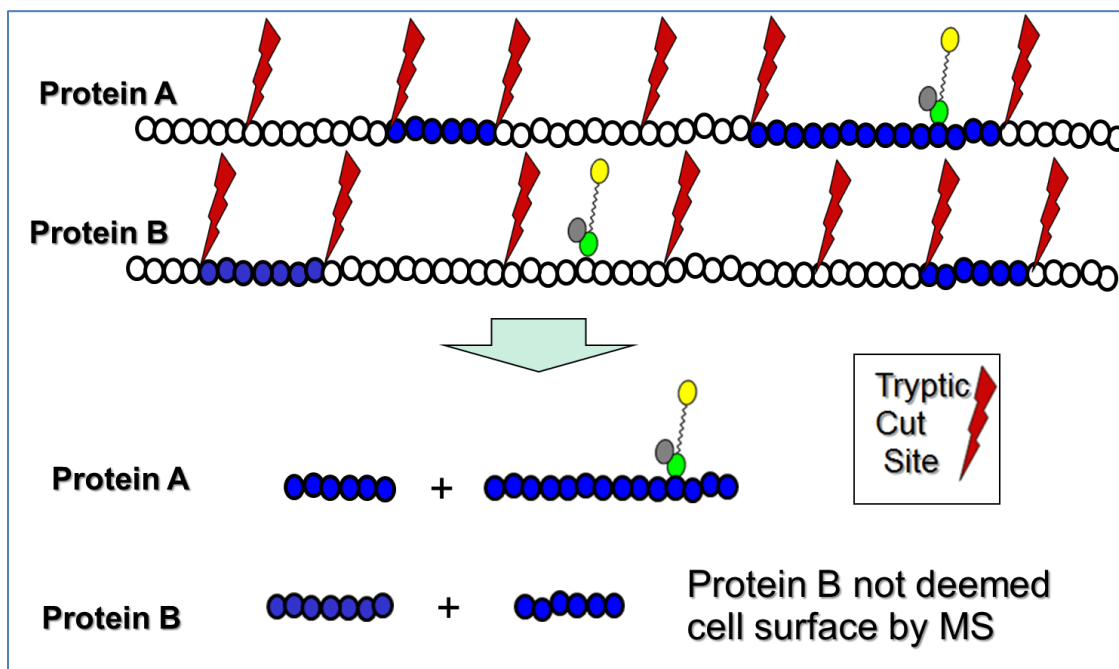
Table 11. Ribosomal proteins, labeled if biotinylated, N/A if not identified in that sample "-" if identified, but not biotinylated.

ID	Description	B5	B13
A0T0Q8	30S ribosomal protein S2, chloroplastic	-	-
A0T0R4	30S ribosomal protein S18, chloroplastic	-	-
A0T0X8	50S ribosomal protein L22, chloroplastic	N/A	-
A0T0Y4	50S ribosomal protein L24, chloroplastic	-	N/A
A0T0Z2	30S ribosomal protein S13, chloroplastic	N/A	-
A0T0Z6	30S ribosomal protein S9, chloroplastic	N/A	-
A0T0Z5	50S ribosomal protein L13	N/A	-
B5YLN7	RL5, ribosomal protein 5, 60S large ribosomal subunit	-	-
B5YMS4	RL3, ribosomal protein 3, 60S large ribosomal subunit	-	-
B5YMU6	RL18, ribosomal protein 18, 60S large ribosomal subunit	-	Biotinylation
B5YNM6	RL21, ribosomal protein 21, 60S large ribosomal subunit	-	Biotinylation
B8BQX6	RS30, ribosomal protein 30 40S small ribosomal subunit	N/A	Biotinylation
B8BS56	RL28, ribosomal protein 28 60S large ribosomal subunit (Fragment)	N/A	-
B8BS57	Ribosomal protein L15	-	Biotinylation
B8BTA9	RS18, ribosomal protein 18 40S small ribosomal subunit	-	Biotinylation
B8BTS3	RL12, ribosomal protein 11 60S large ribosomal subunit	-	-
B8BTT5	Phosphoribosyl pyrophosphate synthetase (EC 2.7.6.1)	-	-
B8BUA7	RL14, ribosomal protein 14 60S large ribosomal subunit	N/A	-
B8BUN1	RS7, ribosomal protein 7	-	Biotinylation
B8BV47	RL7, ribosomal protein 7	-	Biotinylation
B8BVM9	Ribosomal protein L19	-	Biotinylation
B8BVQ0	RL9, ribosomal protein 9	-	-
B8BVV7	RS4, ribosomal protein 4	-	Biotinylation
B8BVY6	RL17A, ribosomal protein 27A 60S large ribosomal subunit	-	-
B8BXX5	RL24, ribosomal protein 24 60S large ribosomal subunit (Fragment)	-	Biotinylation
B8BY08	RL17, ribosomal protein 17-like 60S large ribosomal subunit (Fragment)	-	-
B8BYG9	40S ribosomal protein-like protein	-	-
B8BZ86	RL11A, ribosomal protein 11A 60S large ribosomal subunit	-	-

B8BZD7	RS16, ribosomal protein 16 40S small ribosomal subunit	N/A	Biotinylation
B8BZG7	60S ribosomal protein L18a	-	Biotinylation
B8BZT2	RL34, ribosomal protein 34 60S large ribosomal subunit	-	Biotinylation
B8C0K5	RS13, ribosomal protein 13 40S small ribosomal subunit	-	-
B8C0K6	60S ribosomal protein L13	-	-
B8C0R3	RL13A, ribosomal protein 13A 60S large ribosomal subunit	-	Biotinylation
B8C179	RS10, ribosomal protein 10 40S small ribosomal subunit (Fragment)	N/A	-
B8C1H2	RS9, ribosomal protein 9	-	Biotinylation
B8C1P3	RS11, ribosomal protein 11 40S small ribosomal subunit	-	Biotinylation
B8C1Z7	RS23, ribosomal protein 23 40S small ribosomal subunit	-	-
B8C239	RL4e, ribosomal protein 4e 60S large ribosomal subunit	-	Biotinylation
B8C3Y3	RL10, ribosomal protein 10 60S large ribosomal subunit	-	Biotinylation
B8C5H1	RL22, ribosomal protein 22 60S large ribosomal subunit	-	-
B8C5Y3	RS26, ribosomal protein 26 40S small ribosomal subunit (Fragment)	N/A	-
B8C8U6	RS15A, ribosomal protein 15 40S small ribosomal subunit	N/A	-
B8C8U7	RL35A, ribosomal protein 35A 60S large ribosomal subunit	N/A	Biotinylation
B8C8V8	RS2, ribosomal protein 2	Biotinylation	-
B8C9W9	RL32, ribosomal protein 32 60S large ribosomal subunit	N/A	Biotinylation
B8C9Z4	Protein 23 of the large ribosomal subunit	N/A	-
B8CB96	40S ribosomal protein S8	-	-
B8CBR7	60S ribosomal protein L6 (Fragment)	-	-
B8CC69	RS5, ribosomal protein 5	-	-
B8CCJ1	RS27, ribosomal protein 27 40S small ribosomal subunit	-	-
B8CCL8	40S ribosomal protein S6	-	Biotinylation
B8CCN2	RL8, ribosomal protein 8 (Fragment)	-	Biotinylation
B8CCQ5	RS25, ribosomal protein 25 40S small ribosomal subunit	N/A	-
B8CDP0	40S ribosomal protein S12 (Fragment)	-	-
B8CET5	RS3A, ribosomal protein 3A 40S small ribosomal subunit	-	Biotinylation
A0T0Y1	50S ribosomal protein L29, chloroplastic 1	-	N/A
A0T0Z9	30S ribosomal protein S7, chloroplastic	-	N/A

B8C4E1	ATP phosphoribosyltransferase (EC 2.4.2.17)	-	N/A
B8C5C3	60S ribosomal protein L10A	-	N/A
B8C6V3	Methylthioribose-1-phosphate isomerase (M1Pi) (MTR-1-P isomerase) (EC 5.3.1.23) (S-methyl-5-thioribose-1-phosphate isomerase) (Translation initiation factor eIF-2B subunit alpha/beta/delta-like protein)	-	N/A
B8C8K9	RS1, ribosomal protein 1 (Fragment)	-	N/A
B8CC59	RS29, ribosomal protein 29 40S small ribosomal subunit	-	N/A
B8CDJ9	60S subunit ribosomal protein L27	-	N/A

Table 12. Ribosomal proteins, labeled if biotinylated, "-" if identified but no identified peptides are biotinylated.

ID	Description	B5	B13
A0T0N5	Ribulose-1,5-bisphosphate carboxylase/oxygenase small subunit	Biotinylated	Biotinylated
A0T0P5	Photosystem II CP47 chlorophyll apoprotein	-	-
A0T0S3	ATP-dependent zinc metalloprotease FtsH 1 (EC 3.4.24.-)	-	-
B5YLI4	Argininosuccinate synthase (EC 6.3.4.5)	-	-
B5YLQ5	Mitochondrial chaperonin	-	-
B5YLU3	Fucoxanthin chlorophyll a/c protein-LI818 clade	-	-
B5YMF5	Acetyl-coa carboxylase	-	-
B5YN92	Phosphoglycerate kinase (EC 2.7.2.3)	-	-
B8BQU2	Glyceraldehyde-3-phosphate dehydrogenase (EC 1.2.1.12) (Fragment)	-	Biotinylated
B8BT02	Aspartate aminotransferase (EC 2.6.1.-) (EC 2.6.1.1)	-	-
B8BTJ8	NADPH nitrite reductase (EC 1.7.1.4)	-	-
B8BTR4	Transketolase (EC 2.2.1.1)	-	-
B8BVN3	Pyruvate kinase (EC 2.7.1.40) (Fragment)	-	-
B8BX92	Fucoxanthin chlorophyll a/c protein 6	-	-
B8BY55	S-adenosylmethionine synthase (EC 2.5.1.6)	Biotinylated	Biotinylated
B8BZ41	Phosphofructokinase (EC 2.7.1.90)	-	-
B8BZG0	Ammonia dependent carbamoyl phosphate synthase(EC 6.3.5.5)	-	-
B8BZT6	Pyruvate kinase (EC 2.7.1.40)	-	Biotinylated
B8C0K3	Fucoxanthin chl a/c light-harvesting protein	-	Biotinylated
B8C240	Homoserine dehydrogenase (EC 1.1.1.3)	-	-
B8C246	Triosephosphate isomerase/glyceraldehyde-3-phosphate dehydrogenase (EC 1.2.1.12)	-	-
B8C247	Glyceraldehyde 3-phosphate dehydrogenase	-	-
B8C303	Glyceraldehyde-3-phosphate dehydrogenase	-	-
B8C488	Dihydrolipamide s-acetyltransferase (EC 2.3.1.12)	-	-
B8C4I5	Oxygen-evolving enhancer protein 1	-	-
B8CE42	Pyruvate carboxylase-like protein	-	-
B8CFA9	Ascorbate peroxidase (EC 1.11.1.11)	-	-
B8CFG5	Fucoxanthin chlorophyll a/c protein 4	-	-
B8CGK1	Putative uncharacterized protein GLNN	-	-
B8LBI2	Putative glycine decarboxylase L protein(EC 1.8.1.4)	-	-
B8LEU6	PSAF, photosystem I reaction center subunit (Fragment)	-	-

P93854	Fucoxanthin-chlorophyll a/c light-harvesting protein (Fragment)	-	-

Figure 14. Trypsin cuts after lysine (red) and arginine (orange) to make a variety of peptides from the same section of a protein. The presence of the BR decreases trypsin's ability to cut peptides at that lysine. For example, if the true BPAR of this protein is 50%, biotinylated peptides cut at the biotinylated K (large, bold, red) would be present in reduced numbers, giving BPARs of 23 -29%. Similarly the peptides not cut at the biotinylated K would be present in increased numbers, giving BPARs of 60-63%.
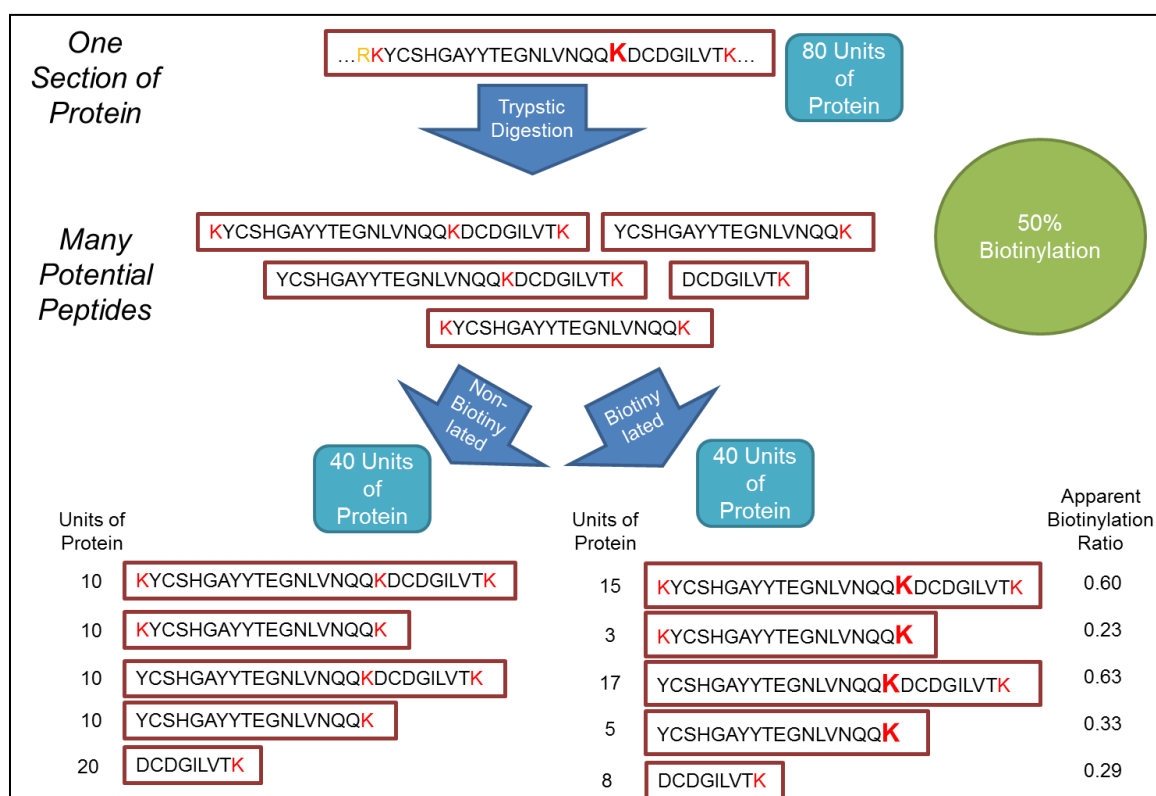
Table 13. Relative quantification of all proteins.

| ID | Description | Log2(N15/N14) | | Mean | SD |
		B13	B5		
A0T096	Photosystem II CP43 chlorophyll apoprotein		-0.18		
A0T0B2	Photosystem II CP47 chlorophyll apoprotein	-0.32			
A0T0K6	Elongation factor Tu, chloroplastic	0.48			
A0T0M8	Photosystem I P700 chlorophyll a apoprotein A1	0.39	0.20	0.29	0.10
A0T0M9	Photosystem I P700 chlorophyll a apoprotein A2	0.57	0.20	0.38	0.18
A0T0N2	Cytochrome c-550	-0.02			
A0T0N5	Ribulose-1,5-bisphosphate carboxylase/oxygenase small subunit	0.32	0.25	0.29	0.03
A0T0P4	ATP synthase subunit alpha, chloroplastic (EC 3.6.3.14) (ATP synthase F1 sector subunit alpha) (F-ATPase subunit alpha)	0.61	0.13	0.37	0.24
A0T0P5	Photosystem II CP47 chlorophyll apoprotein	-0.63	-0.05	-0.34	0.29
A0T0P8	Photosystem II reaction center protein H (PSII-H) (Photosystem II 10 kDa phosphoprotein)	0.59			
A0T0Q8	30S ribosomal protein S2, chloroplastic	0.22			
A0T0R1	DNA-directed RNA polymerase subunit beta (EC 2.7.7.6) (PEP) (Plastid-encoded RNA polymerase subunit beta) (RNA polymerase subunit beta)	1.16			
A0T0R6	ATP synthase subunit beta, chloroplastic (EC 3.6.3.14) (ATP synthase F1 sector subunit beta) (F-ATPase subunit beta)	0.49	0.29	0.39	0.10
A0T0R9	Apocytochrome f	0.20	-0.25	-0.03	0.23
A0T0S0	Magnesium-chelatase subunit I (Mg-protoporphyrin IX chelatase)		0.15		
A0T0S3	ATP-dependent zinc metalloprotease FtsH 1 (EC 3.4.24.-)		0.30		
A0T0T0	Photosystem II D2 protein (PSII D2 protein) (EC 1.10.3.9) (Photosystem Q(A) protein)		-0.23		
A0T0T5	Photosystem I ferredoxin-binding protein (Predicted protein)	0.12			
A0T0T6	Cytochrome b6	-0.10	-0.48	-0.29	0.19

A0T0X0	60 kDa chaperonin, chloroplastic (Protein Cpn60) (groEL protein)		0.26		
A0T0X1	Chaperone protein dnaK (HSP70) (Heat shock 70 kDa protein) (Heat shock protein 70)	0.62	0.04	0.33	0.29
A0T100	Elongation factor Tu, chloroplastic (EF-Tu)		-0.02		
A0T102	ATP-dependent clp protease ATP-binding subunit	0.38	0.67	0.52	0.15
A8DP73	Ribulose-1,5-bisphosphate carboxylase/oxygenase large subunit (Fragment)	0.56	0.17	0.36	0.20
B5YLI4	Argininosuccinate synthase (EC 6.3.4.5)	-0.60	0.04	-0.28	0.32
B5YLN3	Aminopeptidase with a membrane alanine aminopeptidase domain (EC 3.4.11.-)		0.42		
B5YLN7	RL5, ribosomal protein 5, 60S large ribosomal subunit	0.06	-0.05	0.00	0.06
B5YLN9	Predicted protein	-0.03			
B5YLQ5	Mitochondrial chaperonin	0.71	0.09	0.40	0.31
B5YLQ7	Serine hydroxymethyltransferase (EC 2.1.2.1)		0.49		
B5YLU3	Fucoxanthin chlorophyll a/c protein-LI818 clade	-0.73	0.50	-0.12	0.62
B5YLV4	Predicted protein (Fragment)	-1.69	0.27	-0.71	0.98
B5YLX5	copper-induced girdle band-associated cell surface protein precursor	-2.83	1.14	-0.85	1.98
B5YLZ3	Predicted protein	0.32			
B5YM44	Predicted protein	0.27	0.02	0.14	0.12
B5YMD2	Predicted protein (Fragment)	0.97			
B5YMD7	Histone H4	-0.49	-1.96	-1.23	0.73
B5YMF5	Acetyl-coa carboxylase	0.30	1.21	0.75	0.46
B5YMG3	Predicted protein	-0.25			
B5YMN6	Protein scp/tpx-1/ag5/pr-1/sc7 domain-containing protein	0.51			
B5YMQ0	Glutamate 1-semialdehyde 2,1-aminomutase		1.26		
B5YMS4	RL3, ribosomal protein 3, 60S large ribosomal subunit	-0.05	-0.12	-0.09	0.03
B5YMU6	RL18, ribosomal protein 18, 60S large ribosomal subunit	-0.42	-0.50	-0.46	0.04
B5YMV8	Chaperone, heat shock protein 70		0.55		

B5YMW8	Histone H2B	-0.04	-2.02	-1.03	0.99
B5YN39	Aspartate aminotransferase (EC 2.6.1.1)		0.50		
B5YN85	Predicted protein		0.32		
B5YN92	Phosphoglycerate kinase (EC 2.7.2.3)	-0.07	-0.49	-0.28	0.21
B5YN94	Protein scp/tpx-1/ag5/pr-1/sc7 domain-containing protein	0.25			
B5YN96	Protein scp/tpx-1/ag5/pr-1/sc7 domain-containing protein	0.01			
B5YNG5	Predicted protein	-0.30			
B5YNH1	Predicted protein	-0.17			
B5YNI6	Predicted protein		-0.49		
B5YNJ0	Silicic acid transporter, silicon transport		-0.30		
B5YNM6	RL21, ribosomal protein 21, 60S large ribosomal subunit	-0.35	-0.37	-0.36	0.01
B5YNU1	Predicted protein		-0.14		
B5YNX9	Predicted protein (Fragment)	0.04			
B5YNY2	Translation initiation factor IF-2	0.19			
B5YNY5	V-type H-ATPase subunit C (EC 3.6.3.14)		-0.16		
B5YNY9	Predicted protein (Fragment)	-0.17			
B5YP88	ATP synthase subunit beta (EC 3.6.3.14)	-0.03	-0.06	-0.05	0.02
B8BPW0	Putative uncharacterized protein	-0.07	0.23	0.08	0.15
B8BPZ0	Predicted protein	-0.17			
B8BQ15	Chelatase of mg-protoporphyrin IX chelatase		1.19		
B8BQ67	Alkaline phosphatase (EC 3.1.3.1) (Fragment)		-1.27		
B8BQ71	Predicted protein (Fragment)	-0.04			
B8BQ72	Guanine nucleotide binding protein beta subunit-like protein	0.17	0.06	0.12	0.06
B8BQA0	Putative uncharacterized protein (Fragment)	-0.11			
B8BQC2	Malate dehydrogenase (EC 1.1.1.37)		-0.20		
B8BQH4	Predicted protein	-0.39	-0.20	-0.29	0.10
B8BQL0	Heat shock protein belonging to the HSP70 family		-0.09		
B8BQL6	Ftr1_plasma membrane iron permease	-1.06	-1.93	-1.50	0.44
B8BQL7	Putative uncharacterized protein		0.03		
B8BQN4	Predicted protein	-0.03			
B8BQQ3	Predicted protein		0.93		
B8BQR8	Aspartate aminotransferase (asp+ 2 oxoglutarate = OAA +)		0.01		
B8BQT4	Predicted protein		-0.84		
B8BQU2	Glyceraldehyde-3-phosphate dehydrogenase (EC 1.2.1.12)	0.10	0.06	0.08	0.02

	(Fragment)				
B8BQU3	Transketolase (EC 2.2.1.1)		-0.18		
B8BQX6	RS30, ribosomal protein 30 40S small ribosomal subunit	0.29			
B8BQY8	Predicted protein		-0.07		
B8BR03	Putative uncharacterized protein IDH1		-0.32		
B8BR30	Adenine nucleotide translocator; ATP/ADP translocase	-0.64	0.14	-0.25	0.39
B8BR42	Proteasome subunit alpha type (EC 3.4.25.1)		0.00		
B8BRF3	Long-chain-fatty-acid--CoA ligase (EC 6.2.1.3) (Fragment)		-0.45		
B8BRF4	Cation transport ATPase (EC 3.6.3.8)		-0.13		
B8BRG5	Putative uncharacterized protein (Fragment)	0.17			
B8BRH9	HNKH	0.01			
B8BRR6	Tubulin beta		0.31		
B8BRW1	Predicted protein	0.20			
B8BRY1	Predicted protein		0.96		
B8BS06	Precursor of synthetase (EC 6.2.1.4)		-0.47		
B8BS24	Histone H2A (Fragment)	-1.42			
B8BS67	Fucoxanthin chlorophyll a/c protein 8	-0.41			
B8BS69	Predicted protein (Fragment)		-0.63		
B8BS83	Putative uncharacterized protein	-0.01			
B8BSR2	Predicted protein		0.34		
B8BST2	Predicted protein	0.04			
B8BSU5	Predicted protein	-0.20			
B8BSY9	Predicted protein		-0.19		
B8BT02	Aspartate aminotransferase (EC 2.6.1.-) (EC 2.6.1.1)		-0.04		
B8BT14	Predicted protein (Fragment)	-0.05			
B8BT62	Predicted protein	-0.41	0.35	-0.03	0.38
B8BT71	Predicted protein		-0.28		
B8BTA9	RS18, ribosomal protein 18 40S small ribosomal subunit	0.09	-0.47	-0.19	0.28
B8BTC7	Putative uncharacterized protein		-0.95		
B8BTJ8	NADPH nitrite reductase (EC 1.7.1.4)	-0.32	0.80	0.24	0.56
B8BTM0	Predicted protein	0.42			
B8BTM9	Sterol regulatory element-binding protein		-1.07		
B8BTR4	Transketolase (EC 2.2.1.1)	0.26	0.02	0.14	0.12
B8BTT5	Phosphoribosyl pyrophosphate synthetase (EC 2.7.6.1)	-0.60	0.50	-0.05	0.55
B8BTZ3	Predicted protein		-0.02		

B8BU19	Predicted protein		-0.13		
B8BU42	Predicted protein		0.28		
B8BU69	Predicted protein	-0.15			
B8BU77	Predicted protein		0.10		
B8BU95	Predicted protein	-0.37	-0.06	-0.22	0.16
B8BUA7	RL14, ribosomal protein 14 60S large ribosomal subunit	-0.58			
B8BUC2	Predicted protein (Fragment)	-0.29			
B8BUE1	Vacuolar membrane proton pump, inorganic pyrophosphatase (EC 3.6.1.1)		-0.11		
B8BUG6	Niemann-pick C type protein-like protein (Fragment)		0.49		
B8BUJ6	Predicted protein		0.17		
B8BUM6	Dihydrolipoamide s-acetyltransferase (EC 2.3.1.12)		-0.08		
B8BUN1	RS7, ribosomal protein 7	-0.01			
B8BUZ5	Spermidine synthase (EC 2.5.1.16)		-0.13		
B8BV10	Ca2+-dependent membrane-binding protein annexin	-0.99	-0.83	-0.91	0.08
B8BV12	Putative uncharacterized protein		-0.86		
B8BV47	RL7, ribosomal protein 7	-0.10	-0.30	-0.20	0.10
B8BV60	Predicted protein		-0.08		
B8BV79	Putative uncharacterized protein		-0.08		
B8BVC7	2-dehydro-3-deoxyphosphoheptonate aldolase-like protein (EC 2.5.1.54)		0.02		
B8BVG3	Predicted protein		0.23		
B8BVI1	Fucoxanthin-chlorophyll a-c binding protein, plastid	-0.49			
B8BVK5	Atp-dependent RNA DEAD/DEAH box helicase		-0.32		
B8BVM2	Metalloprotease (EC 3.4.24.-) (Fragment)		0.34		
B8BVM7	Elongation factor Ts 1, mitochondrial (EF-Ts 1) (EF-TsMt 1)		0.27		
B8BVN2	Predicted protein	-0.17			
B8BVN3	Pyruvate kinase (EC 2.7.1.40) (Fragment)		-0.11		
B8BVN5	Putative uncharacterized protein		0.23		
B8BVQ0	RL9, ribosomal protein 9		-0.43		
B8BVS4	Predicted protein		0.20		
B8BVT0	Phosphate transport protein	-0.05	0.16	0.05	0.10
B8BVV7	RS4, ribosomal protein 4	-0.28	-0.08	-0.18	0.10
B8BVV8	Predicted protein		-0.26		
B8BW06	Predicted protein	0.57			
B8BWB9	Heat shock protein/chaperone	0.02	-0.06	-0.02	0.04

B8BWG8	ABC transporter		-0.30		
B8BWJ4	Putative uncharacterized protein (Fragment)		-0.40		
B8BWN2	Predicted protein	0.88			
B8BWS1	Predicted protein	1.22			
B8BWS4	Predicted protein	0.99	-0.22	0.39	0.60
B8BX06	14-3-3-like protein	-0.99			
B8BX31	Glycine decarboxylase p-protein		1.25		
B8BX37	Predicted protein		-0.22		
B8BX92	Fucoxanthin chlorophyll a/c protein 6	-0.50			
B8BXA1	Enoyl-reductase [NADH] (EC 1.3.1.9)		-0.21		
B8BXD7	possible ascorbate peroxidase	-0.26			
B8BXD9	Predicted protein		0.24		
B8BXN3	Nitrate transporter	1.79	0.46	1.12	0.67
B8BXN4	Formate/nitrite transporter family member		-0.57		
B8BXS1	Fructose-bisphosphate aldolase (EC 4.1.2.13)		0.33		
B8BXW2	Phosphoglycerate kinase (EC 2.7.2.3)		-0.15		
B8BY22	HNKH	-1.08			
B8BY36	Heat shock protein		0.37		
B8BY55	S-adenosylmethionine synthase (EC 2.5.1.6)	-0.24	0.31	0.04	0.27
B8BY61	Atp-dependent RNA helicase	0.48			
B8BY99	Predicted protein		-0.56		
B8BYC9	Aspartate-semialdehyde dehydrogenase (EC 1.2.1.11)		-0.14		
B8BYD7	Probable isoleucine-trna synthetase (EC 6.1.1.4)		-0.25		
B8BYF6	Predicted protein		-0.42		
B8BYG9	40S ribosomal protein-like protein	0.20	0.06	0.13	0.07
B8BYK3	Predicted protein	-0.17			
B8BYQ5	Predicted protein		-0.05		
B8BYW8	Phosphoenolpyruvate carboxylase (EC 4.1.1.31); cytoplasmic		1.05		
B8BYW9	Predicted protein		0.76		
B8BZ32	Putative uncharacterized protein	-0.23			
B8BZ40	Phosphoribulokinase (EC 2.7.1.19)		0.42		
B8BZ41	Phosphofructokinase (EC 2.7.1.90)	-0.55	-0.43	-0.49	0.06
B8BZ49	Predicted protein	1.18			
B8BZ53	Predicted protein	0.84			
B8BZ86	RL11A, ribosomal protein 11A 60S large ribosomal subunit		-0.28		
B8BZA2	Predicted protein	-0.01	0.53	0.26	0.27

B8BZC2	Inosine-5'-monophosphate dehydrogenase (EC 1.1.1.205)		-0.53		
B8BZD7	RS16, ribosomal protein 16 40S small ribosomal subunit	-0.35			
B8BZE7	Putative uncharacterized protein		0.22		
B8BZG0	Ammonia dependent carbamoyl phosphate synthase(EC 6.3.5.5)	0.98	0.90	0.94	0.04
B8BZG7	60S ribosomal protein L18a	0.32	-0.54	-0.11	0.43
B8BZI8	Predicted protein		-0.06		
B8BZI9	U3 snornp-associated 55-kDa protein	0.00			
B8BZK8	Predicted protein	-0.19			
B8BZQ2	Predicted protein	-0.29			
B8BZQ3	PGR5-like protein		-1.14		
B8BZR6	Predicted protein	0.12			
B8BZR9	Asparagine synthetase (EC 6.3.5.4)		-0.01		
B8BZT2	RL34, ribosomal protein 34 60S large ribosomal subunit		-0.57		
B8BZT6	Pyruvate kinase (EC 2.7.1.40)	-0.73	0.22	-0.25	0.47
B8BZT7	Pyruvate kinase (EC 2.7.1.40)		0.14		
B8BZX6	Heterotrimeric G protein beta subunit 1	0.11			
B8C006	Predicted protein		0.58		
B8C018	Predicted protein		-0.01		
B8C084	Predicted protein	-0.14			
B8C0B6	Predicted protein		-0.53		
B8C0D4	Predicted protein	-0.29	-0.07	-0.18	0.11
B8C0D8	similar to low CO2 inducible membrane protein		2.01		
B8C0D9	similar to low CO2 inducible membrane protein		2.00		
B8C0H0	Importin beta-1 subunit-like protein (Fragment)		0.08		
B8C0K3	Fucoxanthin chl a/c light-harvesting protein		0.51		
B8C0K5	RS13, ribosomal protein 13 40S small ribosomal subunit	0.21			
B8C0K6	60S ribosomal protein L13	-0.29	0.00	-0.15	0.14
B8C0L1	Vacuolar ATPase (EC 3.6.1.3) (EC 3.6.3.14) (EC 3.6.3.6)	0.00	-0.41	-0.21	0.20
B8C0L7	Predicted protein		0.33		
B8C0M3	Predicted protein	0.09	0.45	0.27	0.18
B8C0N4	Predicted protein	-0.25			
B8C0N7	Ferredoxin--NADP reductase (EC 1.18.1.2)	-0.14	-0.22	-0.18	0.04
B8C0Q3	Putative uncharacterized protein		-0.45		

B8C0R3	RL13A, ribosomal protein 13A 60S large ribosomal subunit	0.17	-0.22	-0.02	0.19
B8C0W4	ATP synthase gamma chain	0.48	0.23	0.35	0.12
B8C0Z9	Coatomer protein subunit beta2		-0.44		
B8C135	Predicted protein		-0.24		
B8C140	Phosphoglucomutase (EC 5.4.2.2)		0.36		
B8C141	Putative uncharacterized protein (Fragment)		0.57		
B8C149	Casein kinase-like protein	-0.74			
B8C160	Predicted protein	0.78			
B8C194	Predicted protein	-0.32			
B8C1A4	ABC cassette-containing protein (Fragment)	0.32	0.68	0.50	0.18
B8C1B9	Adenylate cyclase (Fragment)		-0.83		
B8C1C2	Eukaryotic translation initiation factor 3, subunit 10 (Fragment)	0.16	0.29	0.23	0.07
B8C1F9	Ribonuclease (Fragment)	0.10			
B8C1H2	RS9, ribosomal protein 9	-0.10	0.16	0.03	0.13
B8C1L0	Cation transporting ATPase (EC 3.6.3.-) (Predicted protein) (Fragment)	-0.01	0.22	0.11	0.12
B8C1P3	RS11, ribosomal protein 11 40S small ribosomal subunit	0.07	-0.43	-0.18	0.25
B8C1P6	Gdp-d-mannose 4,6-dehydratase (EC 4.2.1.47)		-0.10		
B8C1R6	ATP synthase gamma chain		0.04		
B8C1R7	Phospoenolpyruvate carboxylase (EC 4.1.1.31) (Fragment); mitochondrial		0.48		
B8C1R9	Predicted protein		0.22		
B8C1V2	Putative uncharacterized protein		-0.54		
B8C1V6	Predicted protein (Fragment)	0.41			
B8C1W6	Predicted protein		0.90		
B8C1Z7	RS23, ribosomal protein 23 40S small ribosomal subunit	0.12	-0.51	-0.19	0.31
B8C239	RL4e, ribosomal protein 4e 60S large ribosomal subunit	-0.43	-0.04	-0.23	0.20
B8C240	Homoserine dehydrogenase (EC 1.1.1.3)		0.50		
B8C241	26S proteasome regulatory subunit RPN1 2		-0.05		
B8C246	Triosephosphate isomerase/glyceraldehyde-3-phosphate dehydrogenase (EC 1.2.1.12)	-0.19	0.24	0.02	0.21
B8C247	Glyceraldehyde 3-phosphate dehydrogenase	-0.41	0.86	0.23	0.64
B8C272	Predicted protein	-0.68	-0.31	-0.49	0.19
B8C2A8	Predicted protein	-1.24			

B8C2L6	WD40-repeat protein	0.15			
B8C2N9	V-type h-atpase (EC 3.6.3.14)		-0.21		
B8C2R7	Putative uncharacterized protein (Fragment)	1.59	0.07	0.83	0.76
B8C2W5	Predicted protein		-0.34		
B8C300	Probable bifunctional purine synthesis protein (EC 2.1.2.3)	0.70	-0.15	0.27	0.43
B8C303	Glyceraldehyde-3-phosphate dehydrogenase		-0.36		
B8C306	Predicted protein		-0.08		
B8C359	Acetyl-coenzyme a synthetase (EC 6.2.1.1) (Fragment)		-0.32		
B8C362	Ypt1-like rab-type small G protein		-0.23		
B8C388	Structure specific recognition protein 1	-0.27			
B8C3L2	Putative uncharacterized protein		-0.03		
B8C3M4	HNKH		-0.82		
B8C3P2	Predicted protein	0.70			
B8C3T7	Putative uncharacterized protein		-0.38		
B8C3V9	Aconitase hydratase 2 (EC 4.2.1.3)	0.12	-0.04	0.04	0.08
B8C3X0	DNA-binding protein (Fragment)	0.53			
B8C3Y2	Eukaryotic translation initiation factor 3 subunit 8 (Fragment)	0.60			
B8C3Y3	RL10, ribosomal protein 10 60S large ribosomal subunit	-0.54	0.13	-0.21	0.33
B8C469	Translation factor tu domain 2 (EC 3.6.5.3)	0.07	0.07	0.07	0.00
B8C486	Predicted protein		0.31		
B8C490	Predicted protein (Fragment)	0.13			
B8C4E1	ATP phosphoribosyltransferase (EC 2.4.2.17)		-0.01		
B8C4I5	Oxygen-evolving enhancer protein 1	-0.16	0.07	-0.05	0.12
B8C4Q2	Predicted protein	-1.89	0.07	-0.91	0.98
B8C4Q7	Protein scp/tpx-1/ag5/pr-1/sc7 domain-containing protein	1.18			
B8C4T7	Predicted protein		0.16		
B8C4U8	Predicted protein		-0.09		
B8C553	Adenosylhomocysteinase (EC 3.3.1.1)	-0.01	0.28	0.14	0.14
B8C572	Putative uncharacterized protein	-0.19			
B8C588	Predicted protein (Fragment)	-0.34			
B8C5C3	60S ribosomal protein L10A		-0.17		
B8C5H1	RL22, ribosomal protein 22 60S large ribosomal subunit	0.25			
B8C5I7	Predicted protein	-0.38			
B8C5K0	26S proteasome ATPase regulatory subunit		-0.50		

B8C5P9	Precursor of pyruvate dehydrogenase E1 a		0.18		
B8C5T0	Predicted protein		-0.13		
B8C5Y3	RS26, ribosomal protein 26 40S small ribosomal subunit (Fragment)	0.25			
B8C5Y5	Coatomer protein subunit alpha	0.43			
B8C622	Putative uncharacterized protein		-0.34		
B8C635	Heat shock protein 70	-0.56	-0.15	-0.36	0.21
B8C637	HSP90 family member	-0.24	0.10	-0.07	0.17
B8C680	Predicted protein		0.00		
B8C6C6	ATP synthase subunit alpha	-0.38	-0.16	-0.27	0.11
B8C6H5	Probable serine protease inhibitor	0.47	-0.13	0.17	0.30
B8C6T1	Predicted protein	0.31			
B8C6W4	Predicted protein	-0.25			
B8C712	Predicted protein		0.18		
B8C788	Probable serine protease inhibitor	0.24	1.09	0.67	0.42
B8C789	Probable serine protease inhibitor	0.19	0.34	0.27	0.07
B8C7S8	Putative uncharacterized protein		-0.24		
B8C7S9	Predicted protein	0.17	0.57	0.37	0.20
B8C7U8	Predicted protein	1.34			
B8C7W7	Beta subunit of tetrameric clathrin adaptor complex AP1		-0.11		
B8C832	Tubulin alpha		-0.15		
B8C859	Predicted protein	0.00			
B8C871	Adenosine kinase (EC 2.7.1.20)		0.92		
B8C872	Predicted protein	1.93			
B8C875	Predicted protein		-1.74		
B8C8D3	Predicted protein		-0.50		
B8C8H3	Predicted protein	-0.03			
B8C8K9	RS1, ribosomal protein 1 (Fragment)		0.68		
B8C8L2	Synthase of ATP synthase (EC 3.6.3.14)		0.21		
B8C8L4	Myosin light chain kinase (EC 2.7.11.17) (EC 2.7.11.18)		-0.30		
B8C8L9	Putative uncharacterized protein		0.09		
B8C8N1	Putative uncharacterized protein (Fragment)	-0.01			
B8C8R2	Predicted protein	0.79	1.34	1.07	0.28
B8C8T3	SUPT6H,-like protein to suppressor of ty 6	-0.01			
B8C8T5	Glutamine dependent Carbamoyl phosphate synthase like protein	1.33	1.07	1.20	0.13
B8C8U3	Urea transporter	2.31	-0.32	1.00	1.32
B8C8U6	RS15A, ribosomal protein 15 40S small ribosomal subunit	-0.06			

B8C8U9	Clathrin heavy chain	0.49	-0.05	0.22	0.27
B8C8V1	Predicted protein	-0.60			
B8C8V5	Synaptobrevin (Fragment)		-1.36		
B8C8V8	RS2, ribosomal protein 2	0.46	-0.19	0.14	0.32
B8C920	Predicted protein (Fragment)	0.44			
B8C995	Translation elongation factor alpha (EC 3.6.5.3)	0.32	-0.27	0.03	0.30
B8C9K4	Predicted protein	-0.22			
B8C9M7	Serine threonine protein kinase (Fragment)	-0.35			
B8C9R3	Putative uncharacterized protein	0.48	0.20	0.34	0.14
B8C9X1	5-methyltretrahydrofolate-homocysteine s-methyltransferase (EC 2.1.1.13)	0.87	0.23	0.55	0.32
B8C9Z4	Protein 23 of the large ribosomal subunit	-0.18			
B8CA11	ABC transporter multi-drug efflux transporter-like protein (Fragment)		-1.02		
B8CA58	Predicted protein	-0.03			
B8CAB9	Predicted protein (Fragment)	0.28	-0.81	-0.26	0.54
B8CAG8	Predicted protein	0.03	0.35	0.19	0.16
B8CAP0	Predicted protein	0.13			
B8CAS8	Copper induced cell-surface protein	1.12			
B8CAU5	copper induced cell-surface protein	1.86			
B8CAV0	Copper induced cell-surface protein	1.46			
B8CB37	Coatomer subunit gamma	0.39	-0.12	0.14	0.25
B8CB74	Mucin associated surface protein	0.74			
B8CB96	40S ribosomal protein S8	-0.22	-0.11	-0.17	0.05
B8CBA7	Predicted protein		0.66		
B8CBB2	Protein scp/tpx-1/ag5/pr-1/sc7 domain-containing protein	1.68			
B8CBC2	Predicted protein	0.41			
B8CBE4	Predicted protein	0.09	-0.29	-0.10	0.19
B8CBI7	Predicted protein		0.21		
B8CBN8	Predicted protein (Fragment)	-0.18	0.10	-0.04	0.14
B8CBQ8	Predicted protein	-0.66			
B8CBQ9	Predicted protein		-0.38		
B8CBR7	60S ribosomal protein L6 (Fragment)	-0.26			
B8CBV3	Vacuolar proton pump alpha subunit (EC 3.6.3.14)		-0.26		
B8CBZ5	Predicted protein		-0.57		
B8CC14	Putative uncharacterized protein	-0.51			
B8CC33	Eukaryotic translation initiation factor 4A	-0.57	-0.60	-0.59	0.01
B8CC69	RS5, ribosomal protein 5	0.00	-0.15	-0.07	0.07
B8CC85	Coatomer COPII (Fragment)	0.42			
B8CCA0	Aspartate-ammonia ligase (EC 6.3.1.1)		0.02		

ID	Description				
B8CCA3	Predicted protein	0.68	1.02	0.85	0.17
B8CCA5	UDP-glucose 6-dehydrogenase (EC 1.1.1.22)		-0.22		
B8CCE1	Psedouridylate synthase (EC 4.2.1.70)		0.16		
B8CCE8	Predicted protein	0.48			
B8CCH2	no nearest neighbors		0.49		
B8CCH4	Predicted protein		-0.32		
B8CCJ1	RS27, ribosomal protein 27 40S small ribosomal subunit	0.25			
B8CCL3	Phosphoadenosine-phosphosulphate reductase		0.09		
B8CCL8	40S ribosomal protein S6	-0.13	-0.13	-0.13	0.00
B8CCM1	Predicted protein	-0.13			
B8CCN2	RL8, ribosomal protein 8 (Fragment)	-0.32	-0.13	-0.23	0.09
B8CCQ0	Predicted protein	-0.06			
B8CCS6	Serine hydroxymethyltransferase (EC 2.1.2.1); serine glyoxylate aminotransferase		0.01		
B8CCU2	Putative uncharacterized protein (Fragment)		-0.04		
B8CCV5	Histone H1	0.42			
B8CDB2	Putative uncharacterized protein		0.10		
B8CDB3	Putative uncharacterized protein	-0.04	0.95	0.46	0.50
B8CDI0	long-chain acyl-CoA synthetase-like protein	-0.80			
B8CDJ9	60S subunit ribosomal protein L27		-0.48		
B8CDL6	AMP yield acyl coA synthetase		0.07		
B8CDW8	Glutamine fructose 6 phosphate transaminase (EC 2.6.1.16)		0.40		
B8CE01	Glutamate synthase (EC 1.4.7.1)		0.49		
B8CE42	Pyruvate carboxylase-like protein	0.99	1.00	1.00	0.01
B8CE49	Predicted protein	0.74			
B8CE50	Oligopeptidase (EC 3.4.24.70)		0.01		
B8CE77	Phosphoribosylformylglycinamidine synthase (EC 6.3.5.3)		-0.03		
B8CEC4	Nitrate reductase	-0.23			
B8CEE0	3-isopropylmalate dehydratase (EC 4.2.1.33)		0.36		
B8CEG2	Citrate synthase		0.01		
B8CEN4	Tryptophane synthase (EC 4.2.1.20)		-0.12		
B8CET1	Putative uncharacterized protein	0.73	0.19	0.46	0.27
B8CET5	RS3A, ribosomal protein 3A 40S small ribosomal subunit	-0.11	0.36	0.13	0.24
B8CEV5	Fucoxanthin chlorophyll a/c protein 5	0.26			
B8CF92	Predicted protein		0.03		

B8CFD1	Member of the clp superfamily, regulatory beta subunit		-0.61		
B8CFG3	Predicted protein		0.51		
B8CFG4	Predicted protein	-0.14			
B8CFN3	Predicted protein		-0.46		
B8CFU7	Polyadenlyte binding protein (Fragment)	0.23	0.37	0.30	0.07
B8CFV4	Actin-like protein	-1.04	-0.14	-0.59	0.45
B8CFW3	Fucoxanthin chlorophyll a/c protein 1 (Fragment)	-0.20			
B8CFY7	Predicted protein		-0.28		
B8CFZ9	Glutamine synthetase (EC 6.3.1.2)	-0.37	0.73	0.18	0.55
B8CG46	Predicted protein	0.06	0.28	0.17	0.11
B8CG50	Predicted protein		-0.53		
B8CG56	Putative uncharacterized protein (Fragment)	-0.04			
B8CG69	Predicted protein	0.07			
B8CG95	Predicted protein	0.71			
B8CGE1	Predicted protein	0.52	-0.19	0.16	0.35
B8CGE6	Predicted protein	0.98			
B8CGG0	Fucoxanthin chlorophyll a/c protein, LI818 clade		-0.23		
B8CGH5	N-acetylornithine aminotransferase		0.25		
B8CGJ9	40S ribosomal protein S28		-1.12		
B8CGK1	Putative uncharacterized protein GLNN	0.61	-0.16	0.22	0.39
B8CGK8	Putative uncharacterized protein (Fragment)		-0.15		
B8CGL7	Predicted protein		-0.23		
B8CGL9	Ferredoxin--NADP reductase (EC 1.18.1.2)		0.21		
B8CGM4	Predicted protein		0.36		
B8CGR0	Predicted protein	0.40	1.55	0.98	0.57
B8LBI2	Putative glycine decarboxylase L protein(EC 1.8.1.4)	0.04	-0.27	-0.12	0.16
B8LBP1	26S proteasome regulatory subunit Rpn2 26S subunit, non-atpase		0.10		
B8LBX7	Predicted protein	-0.29			
B8LC25	Predicted protein (Fragment)	0.23			
B8LCI4	Predicted protein		0.38		
B8LCQ7	Predicted protein	0.34			
B8LE04	Iron starvation induced protein		-2.98		
B8LE80	Predicted protein		0.29		
B8LE89	Predicted protein		-1.48		
B8LEA2	Predicted protein	0.86			
B8LEH9	Predicted protein	0.38			

B8LEL7	Nickel ABC transporter, periplasmic nickel-binding protein		2.38		
B8LEM4	Predicted protein	-0.01			
B8LEM5	Predicted protein	-0.03			
B8LEM7	Predicted protein	1.79			
B8LEN2	Predicted protein	1.41			
B8LEP1	Predicted protein	0.56	-0.35	0.11	0.46
B8LEU2	Rubisco expression protein, plastid protein		-0.11		
B8LEU9	Predicted protein	-0.38	0.05	-0.16	0.21
P93853	Fucoxanthin-chlorophyll a/c light-harvesting protein (Fragment)	-0.69	-0.87	-0.78	0.09
P93854	Fucoxanthin-chlorophyll a/c light-harvesting protein (Fragment)	-0.53	-0.47	-0.50	0.03
Q0ZUJ5	Copper expressed protein 15	-0.26			

VITA

Ashley M. New

1984	Born July 25th, Norfolk, VA.
2002-2005	Attended Virginia Polytechnic Institute and State University, Blacksburg, Virginia.
2005	B.S. in Environmental Science, Virginia Polytechnic Institute and State University, Blacksburg, Virginia.
2006-2008	Research specialist, The College of William & Mary, Virginia Institute of Marine Science, Topping, Virginia.
2008-2012	Laboratory researcher, Rutgers University, Newark, New Jersey
2010-2013	M.S. Student, Rutgers University, Newark, New Jersey
2012-2013	Laboratory technician, William Paterson University, Wayne, New Jersey

.

Abstracts

Jones, B. M., Sahin, M. S., New, A. M., Kuska, A. B., 2013. Integrating physiology and 3rd generation DNA sequencing to characterize the effect of MCDW, iron and ligands on Ross Sea eukaryotic phytoplankton assemblages. ASLO, Aquatic Sciences Meeting, SS51, 11872.

Kustka , A. B., Reinfelder, J. R., Gates, C., New, A. M., Bidle, K. D., Milligan, A. J., 2013. The metabolic response of diatoms to low co2 includes c4-assisted photosynthesis and recovery of photorespiratory products: implications for bloom sustenance. ASLO, Aquatic Sciences Meeting, SS80, 12076.

New, A. M., Zheng, H., Kustka A. B., 2012. Investigating Fe acquisition proteins in *Thalassiosira pseudonana* by cell surface biotinylation coupled with mass spectrometry. Ocean Sciences Meeting, SS057, 12872.